MICROVASCULAR OXYGEN TRANSPORT: DEVELOPMENT OF AN OPTICAL TRIPLICATOR

by

Elizabeth A. Mott

Thesis submitted to the Faculty of the

Virginia Polytechnic Institute and State University

in partial fulfillment of the requirements for the degree of

Master of Science

in

Electrical Engineering

APPROVED:

J. Wallace Grant, Co-Chairman

Richard Claus, Co- Chairman

Daniel Schneck

Roland Pittman

August 1992

Blacksburg, Virginia

c.2

MICROVASCULAR OXYGEN TRANSPORT DEVELOPMENT OF AN OPTICAL TRIPLICATOR

(ABSTRACT)

Microvascular oxygen transport has been studied using many experimental methods. The three wavelength photometric method of Pittman and Duling (6) was the basis for this project. An optical triplicator was introduced into the microscopy assembly. The triplicator's function was to take the image seen in the eyepiece of the microscope, triplicate it, filter it at three known wavelengths and direct each image onto the active area of a video camera. When used in-vivo, the triplicator allowed for three simultaneous intensity measurements, one at each wavelength, to be made. This measurement removed any assumptions concerning the uniformity of the blood sample which was inherent in Pittman and Duling's design. Measurements were performed in vivo on several hamster retractor muscles. The intensity information obtained was then used to calculate oxygen saturation at regions near an arterial bifurcation. Oxygen saturation values ranged from 42.99 ± 4.20 to 96.46 ± 4.46% depending upon the location along the vessel. It was also concluded that the oxygen saturation profile across the vessel was altered near a bifurcation. The oxygen saturation profile prior to and following a bifurcation appeared to be uniform. However, in the region of a bifurcation, the asymmetry introduced non-uniformities in the profile.

This paper briefly discusses the theory behind the three wavelength photometric method, the development and fabrication of the optical triplicator and the measurement techniques used to obtain oxygen saturation profiles. It will be shown that the optical triplicator has the potential to advance the study of microvascular oxygen transport beyond previously unachievable levels.

ACKNOWLEDGEMENTS

The completion of this project would have been impossible without the assistance of many people to whom I greatly appreciate. Dr. J. Wallace Grant, my major professor, graciously took me under his supervision and introduced me to Dr. Roland Pittman at the Medical College of Virginia. Dr. Pittman introduced me to microvascular oxygen transport experimentation, provided the necessary experimental equipment and provided his unending support throughout the entirety of the project. It is my sincerest hope that this project will find utility and application in his future work. The aid and expertise of the Fiber and Electro-Optic Research Center, especially Dr. Richard Claus and Dr. Kent Murphy, during the preliminary phases was also invaluable. Bob Davis and the staff in the ESM machine shop were extremely helpful in the development phase. In addition, I would like to thank Dr. Peter Trower for his added assistance with the optical phases of the project and Dr. T. C. Poon who allowed me to utilize his image processing system.

I would like to express my deepest love and gratitude to my family who provided me with love and support throughout my entire college career. And, I would like to dedicate this thesis to my love, Bryan, and thank him for all of his help and support throughout the project.

TABLE OF CONTENTS

1.0 Microvascular Oxygen Transport 1
1.1 Introduction 1
1.2 Literature Review 1
1.3 Problem Formulation 3
1.4 Overview 5

2.0 Three Wavelength Photometric Method 6
2.1 Theoretical Development of Oxygen Saturation for a Solution Containing Oxy- and Deoxyhemoglobin 6
2.2 Theoretical Development of Equations to Determine Oxygen Saturation of Whole Blood . 8
2.3 Selection of Wavelengths 11
2.4 Practical Use of Equation in Experimental Work 12
2.5 Conclusions 16

3.0 Optical Triplicator 17
3.1 Introduction 17
3.2 Optical Triplicator Design 17
3.3 Beamsplitters and Prisms 21
3.4 Interference Filters 22
3.5 Redirection of Triplicated Images 32
3.6 Overall Design Consideration 34
3.7 Design Conclusions 38

4.0 Fabrication of Optical Triplicator 40
4.1 Introduction 40
4.2 Design of Housing for Optical Triplicator . . 40
4.3 Placement of Optical Elements 47
4.4 Fabrication Conclusions 50

5.0 Data Collection Using Video Microscopy System With Triplicator 51
5.1 Introduction 51
5.2 Video Microscopy System 52
5.3 Image Analysis System 56
5.4 Experimental System Preparation 61
5.5 Hemoglobin Solutions - In Vitro 62
5.6 In Vivo Measurements 69
5.7 Experimental Conclusions 74

6.0 Calculations and Results 77
6.1 Introduction 77
6.2 Hemoglobin Solution Results 77
6.3 Diameter of Retractor Muscle Arteriole Calculations 79

6.4 Hamster Retractor Muscle Oxygen Saturation Calculations 80
6.5 Conclusions 89

7.0 Conclusions and Future Work 93
7.1 Introduction 93
7.2 Observations and Recommendations 93
7.3 Conclusions 95

References 97

Appendix. 99

Vita. 100

LIST OF ILLUSTRATIONS

Figure 1. Preliminary Design of Optical Triplicator . . . 18

Figure 2. Operating Design of Optical Triplicator 20

Figure 3. Orientation of Image Through the System 23

Figure 4. A Bandpass Filter Spectrum 25

Figure 5. Spectrophotometer Readout for 560 nm Bandpass Filter (Omega) 27

Figure 6. Spectrophotometer Readout for 549 nm Bandpass Filter (Omega) 28

Figure 7. Spectrophotometer Readout for 523 nm Bandpass Filter (Omega) 29

Figure 8. Dependency of the Slit Size on the Size of the Active Area and the Maximum Size Vessel to be Viewed (100 μm) 33

Figure 9. Optical Triplicator 35

Figure 10. Single-slit Fraunhofer Diffraction (Hecht) . . 37

Figure 11. Housing for Optical Triplicator 41

Figure 12. Optical Triplicator Mounted Between Microscope and Video Camera 43

Figure 13. Interference Filter Holder 44

Figure 14. Slit Design 46

Figure 15. Optical System and Video System 53

Figure 16. Image Analysis System 57

Figure 17. Example of Plot Generated Using IMAGELAB Software in the Digitizing Mode Using Line Segments 59

Figure 18. Linearity of SIT Camera at 560 nm 64

Figure 19. Three Microslide Hemoglobin Solutions on the Microscope Stage 67

Figure 20. Triplicated Image of an Oxyhemoglobin Solution at Three Wavelengths 68

Figure 21. Hamster Positioned on the Microscope Stage . . 71

Figure 22. Measurement Sites Along an Arteriole Near a Bifurcation 72

Figure 23. Example of Triplicated Image of an Arteriole in a Hamster Retractor Muscle 75

Figure 24. Oxygen Saturation Profile 91

LIST OF TABLES

Table 1. Spectral Characterisitics for Three Bandpass Filters 30

Table 2. Linearity of Dage/MTI Model 66 SIT Camera at 560 nm 63

Table 3. Diameter of Hamster Arteriole 81

Table 4. Intensity Data for Measurement Site 1 82

Table 5. Intensity Data for Measurement Site 2 84

Table 6. Intensity Data for Measurement Site 3 86

Table 7. Intensity Data for Measurement Site 4 87

Table 8. Intensity Data for Hamster Breathing 100% O_2 89

1.0 MICROVASCULAR OXYGEN TRANSPORT

1.1 Introduction

The key to cellular energetics in mammals is the continuous diffusion of oxygen from the vascular system to the tissues. The vascular system is comprised of blood vessels which are broken down into the arterial and venous systems. The arterial system is responsible for delivering oxygenated blood to the muscles and organs of the body. The venous system returns the deoxygenated blood to the heart where, by involving the pulmonary system, the blood is oxygenated. According to Krogh (1), the capillary bed, which lies deep within the tissues therefore bringing the blood close to the cells, is where diffusion of oxygen to the cells takes place.

1.2 Literature Review

In 1957, Davies and Bronk (2) raised the question, opposing the classical theory of Krogh: Where does the majority of oxygen diffusion take place, in the arterioles, capillaries or venules? Krogh believed that the majority of oxygen is transported to the tissue by passive diffusion, caused by gradients in oxygen tension across the capillary walls. Utilizing polarographic oxygen microcathodes, Davies and Bronk were able to show that gradients in oxygen tension were present at the walls of arterioles and venules in the cerebral circulation. Pittman and Duling (3) began their work using photometric techniques to verify this observation.

Using photometric methods on arterioles in the hamster retractor muscle, they were able to measure the oxygen saturation of red blood cell (RBC) hemoglobin (Hb) verifying that some passive diffusion does occur at the arteriolar level.

The photometric method used by Pittman and Duling was a three wavelength quantitative microscopy method. With this method, the optical density of flowing blood at two isosbestic wavelengths for hemoglobin is determined. An isosbestic wavelength is one at which the oxy- and deoxyhemoglobin have equal light absorption. The third wavelength used for optical density measurements, the measuring wavelength, is one which is chosen to have a large difference in oxy- and deoxyhemoglobin light absorption. The optical densities, measured at the isosbestic wavelengths, are used to determine the amount of light scattering off the RBC's. A ratio of the optical density at the measuring wavelength, corrected for scattering, to the optical density at one of the isosbestic wavelengths, also corrected for scattering is used to determine the oxygen saturation. These optical densities are determined along the light path through the vessel. Hence, the calculations depend upon the geometric cross section of the vessel, the spatial uniformity of the RBC's and the velocity profile of the RBC's.

1.3 Problem Formulation

Pittman, along with his colleagues continued using the photometric methods to determine other quantities necessary to assess oxygen transport in microvessels, such as: RBC velocity, vessel diameter, Hb concentration and hematocrit (4, 5, 6, 7). Revisions to the microscopy system described by Pittman and Duling (6) occurred in order to have a computerized task specific system (8). This system was developed based upon the need to measure light intensity and image dimensions simultaneously at several locations in the microscope field and the need for on-line computational capabilities. To incorporate these requirements, the photometric system was modified by using fiber optics to split the light transmitted through an arteriole into three beams. The image then passed through three separate bandpass interference filters and into photomultiplier tubes. The photomultiplier tubes were used for their fast time response characteristics so that continuous measurements could be made.

Although this method was an improvement over the previous methods using a single transmitted beam and sequentially inserting the interference filters, limitations still existed. The previous methods were limited by the time required to change the interference filters. This act could not be performed quickly enough to obtain information on the same blood sample. The bounds of the fiber optic computerized

system lie in the system design. The fiber optic pick-up leads, which bring the light from the microscope to the photomultiplier tubes, were such that only point measurements could be made. Hence, lumenal variations of SO_2 could not be measured. Ineludible assumptions were therefore incorporated into the system. Measurements were made at several points along the centerline of the microvessel, therefore involving the following assumptions:

(1) axially symmetric blood flow through a vessel of circular cross-section (Poiseuillian flow)

(2) red blood cells (and, hence [Hb]) and oxygen are uniformly distributed across the microvessel

Pittman and Ellsworth (7) discovered that RBC's and oxygen are not uniformly distributed across the microvessel. These observations also showed that the blood flow velocity profile was not axially symmetric, or Poiseuillian, but that it was actually blunter than the assumption allowed for.

In order to overcome these bounds inherent in this design, a new design was necessary. The design needed to allow for simultaneous intensity measurements at three different wavelengths along with the ability to measure, also simultaneously, the intensities at several locations across the cross-section of the microvessel. This would yield profile information for Hb and SO_2 concentrations across the microvessel, therefore, not relying on a single centerline

value and a faulty assumption of uniformity. Hence, the development of the optical triplicator.

The optical triplicator simultaneously produces three copies of the image viewed through the eyepiece of the microscope at three different wavelengths. It also directs these images into a video camera which feeds a monitor and a video recorder. During the measurement procedures, a video recording is made for subsequent analysis.

1.4 Overview

The following sections serve as a presentation of the optical triplicator design, fabrication and use. Chapter 6 also includes some results of SO_2 profiles along an arteriole near a bifurcation in the hamster retractor muscle. It will be shown that the optical triplicator promoted this photometric method to a level at which many advances in the theory of oxygen transport to the tissue can be made.

2.0 THREE WAVELENGTH PHOTOMETRIC METHOD

2.1 Theoretical Development of Oxygen Saturation for a Solution Containing Oxy- and Deoxyhemoglobin

The theory of the three wavelength photometric method of Pittman and Duling began by looking at the relationships between transmitted intensity and extinction coefficients according to the Lambert-Beer-Bouguer Law (9). This law is followed by solutions containing a mixture of oxy- and deoxyhemoglobin. It reads that for monochromatic incident light of wavelength λ, the transmitted intensity is:

$$I_t = I_o \, 10^{-\varepsilon_\lambda c d} \qquad (2.1\text{-}1)$$

where: I_t = transmitted intensity

I_o = incident intensity

ε_λ = extinction coefficient ($mM^{-1}\ cm^{-1}$)

c = concentration of Hb (mM)

d = optical path length (cm)

Expressing this equation in terms of optical density,

$$OD = \log \frac{I_o}{I_t} \qquad (2.1\text{-}2)$$

yields an equation proportional to the extinction coefficient,

$$OD_\lambda = \varepsilon_\lambda cd$$

(2.1-3)

The extinction coefficient is related directly to the ability of a substance to absorb light. Therefore, the total extinction coefficient for a solution containing oxy- and deoxyhemoglobin is:

$$\varepsilon_\lambda = SO_2\ \varepsilon_\lambda^1 + (1 - SO_2)\,\varepsilon_\lambda^\circ$$

(2.1-4)

where: ε_λ = extinction coefficient of the mixture

SO_2 = oxygen saturation

ε_λ^1 = extinction coefficient of oxyhemoglobin

$\varepsilon_\lambda^\circ$ = extinction coefficient of deoxyhemoglobin

Hence, to determine oxygen saturation, the optical density of the solution can be measured at two different wavelengths. The first wavelength λ_m, the measuring wavelength, is chosen so there is a large difference between ε_λ^1 and $\varepsilon_\lambda^\circ$. The second wavelength, λ_I, the isosbestic wavelength, is chosen where ε_λ^1 and $\varepsilon_\lambda^\circ$ are equal. Therefore, using equation 2.1-3, at these two wavelengths yields:

$$OD_{\lambda_m} = [SO_2\ \varepsilon_{\lambda_m}{}^1 + (1-SO_2)\ \varepsilon_{\lambda_m}{}^\circ]\ cd$$

(2.1-5a)

and,

$$OD_{\lambda_I} = \varepsilon_{\lambda_I} cd$$

(2.1-5b)

Solving equations 2.1-5a and 2.1-5b for oxygen saturation yields a linear relationship:

$$SO_2 = m\left(\frac{OD_{\lambda_m}}{OD_{\lambda_I}}\right) + b$$

(2.1-6)

where: m = slope =

$$\frac{\varepsilon_{\lambda_I}}{(\varepsilon_{\lambda_m}{}^1 - \varepsilon_{\lambda_m}{}^o)}$$

b = intercept =

$$-\frac{\varepsilon_{\lambda_m}{}^o}{(\varepsilon_{\lambda_m}{}^1 - \varepsilon_{\lambda_m}{}^o)}$$

2.2 Theoretical Development of Equations to Determine Oxygen Saturation of Whole Blood

Equation 2.1-6 allows the oxygen saturation of an oxy-, deoxyhemoglobin solution to be calculated. However, optical properties of whole blood and oxy-, deoxyhemoglobin solutions are significantly different. According to Kramer et al (10) the Lambert-Beer-Bouguer law is not representative of solutions containing RBC's. This is because the RBC's act as scattering centers in the solution. Therefore, a solution of

whole blood has three major factors which control the transmission of light: (1) the scattering of light off the RBC's, (2) the absorption of light by the oxy- and deoxyhemoglobin molecules, and (3) the absorption of light by the plasma. Factors 2 and 3 are also present in an oxy-, deoxyhemoglobin solution; where the plasma would be the saline used to suspend the hemoglobin molecules. Therefore, to assess a whole blood solution, the scattering effects and absorption effects need to be separated.

In 1970, Twersky (11), a mathematician, developed an equation for the transmittance in which the effects due to absorption and scattering are separable. The absorption effects still follow the Lambert-Beer-Bouguer law. The scattering effects depend logarithmically upon the optical path length, hematocrit, wavelength, and particle size, shape and orientation. The development of this complicated scattering dependence is documented in Twersky's paper. For the present discussion, this scattering term will be referred to as B. Hence, the optical density of whole blood can be represented as:

$$OD = \varepsilon c d + B \qquad (2.2\text{-}1)$$

To obtain a linear relationship for oxygen saturation of whole blood, the optical density in the above equation must be

corrected for scattering. Assuming the value for B could be measured or calculated, it could be subtracted from the optical density to give the calculated absorption:

$$OD - B = \varepsilon cd \tag{2.2-2}$$

Measuring optical density under the same physical conditions at two isosbestic wavelengths would allow for the scattering term, B, to be determined. It must be assumed that the scattering terms at each of the isosbestic wavelengths are equal:

$$B = B_{I_1} = B_{I_2} \tag{2.2-3}$$

where B_{I_1} = scattering due to isosbestic wavelength λ_{I_1}

B_{I_2} = scattering due to isosbestic wavelength λ_{I_2}

Solving equation 2.2-2 for B at each isosbestic wavelength yields:

$$B = \frac{(\frac{\varepsilon_{I_1}}{\varepsilon_{I_2}})\, OD_{I_2} - OD_{I_1}}{(\frac{\varepsilon_{I_1}}{\varepsilon_{I_2}}) - 1} \tag{2.2-4}$$

Recall, $\varepsilon_{I_1}/\varepsilon_{I_2}$ is a ratio of extinction coefficients which can be determined using hemoglobin solutions and must be significantly different from 1. Now, introducing a third wavelength, λ_m, the measuring wavelength, the linear relationship for oxygen saturation can be established. Recall, this measuring wavelength is chosen such that there is a large difference between the extinction coefficients of oxy- and deoxyhemoglobin; and it must be chosen close to the isosbestic wavelengths so the scattering term can be assumed to be the same. The linear relation for oxygen saturation would then be:

$$SO_2 = m\left(\frac{OD_{\lambda_m} - B}{OD_{\lambda_r} - B}\right) + b \qquad (2.2\text{-}5)$$

2.3 Selection of Wavelengths

The above development of the oxygen saturation equation discusses the use of three wavelengths, two isosbestic and a measuring wavelength. To determine these wavelengths, spectral characteristics of oxy- and deoxyhemoglobin need to be determined. Most important is the determination of the extinction coefficients over the spectrum.

A second consideration in the selection of the wavelengths is the photometric error. To achieve accurate

optical density measurements, the photometric error must be minimized. This photometric error is mainly due to the type of detector being used. However, to reach minimum photometric error, a wavelength must be chosen so that the product, εcd, is near the optimum optical density (9). For a given hemoglobin concentration, c, the optical path length, d, can be varied at many wavelengths to determine which length produces the lowest photometric error. Van Assendelft (12) who performed a similar calculation showed that 5 to 200 μm vessel diameters, or path lengths can be used with wavelengths in the 400 to 600 nm range to determine the optical density.

Therefore, combining these two considerations and choosing two isosbestic and one measuring wavelength in the 400 to 600 nm range was performed (9). The isosbestic wavelengths chosen were 523 and 549 nm and the measuring wavelength was chosen to be 560 nm.

2.4 Practical Use of Equations in Experimental Work

Section 2.2 described the theoretical development of the oxygen saturation equation (2.2-5). In practice however, this equation is used in a particular manner to determine oxygen saturation values. It must also be noted that using the following method requires that the wavelength and oxygen saturation dependence of B be negligible. If this were not the case, the oxygen saturation relationship would not be linear.

Experimental work must begin using oxy- and deoxyhemoglobin solutions. A distilled water sample must also be incorporated in order to obtain approximate incident intensity, I_o, values. Transmitted intensity values are determined at each of the three wavelengths (λ_{I_1} =549, λ_{I_2} =523, λ_m=560) for the oxy- and deoxyhemoglobin solutions.

Using this information, the following constants are calculated and are used to determine oxygen saturation in whole blood:

$$\rho = \frac{OD_{549}}{OD_{523}} \qquad (2.4\text{-}1a)$$

$$R_1 = \frac{OD_{560}}{OD_{549}} \qquad (2.4\text{-}1b)$$

$$R_0 = \frac{OD_{560}}{OD_{523}} \qquad (2.4\text{-}1c)$$

where subscripts 1 and 0 represent oxy- and deoxyhemoglobin, respectively. Recall, optical density,

$$OD=\log\frac{I_o}{I_t}$$

(2.1-2)

When calculating ρ, typically a ρ_1 for oxyhemoglobin and a ρ_o for deoxyhemoglobin are calculated and averaged to give an overall ρ value.

Next, the linear constants m (slope) and b (intercept) are calculated using the R_1 and R_o values:

$$m=\frac{1}{R_1 - R_0}$$

(2.4-2a)

$$b=\frac{-R_0}{R_1 - R_0}$$

(2.4-2b)

These equations are obtained by simultaneously solving two oxygen saturation equations and allowing SO_2 to equal 1 (i.e. 100%) for oxyhemoglobin and 0 (i.e. 0%) for deoxyhemoglobin.

Following the determination of the constants ρ, m and b, a whole blood sample or an in vivo measurement can be performed. It is necessary to measure transmitted intensity values at each of the three wavelengths. Incident intensity values must also be measured. Approximate in vivo values are measured by measuring the transmitted intensity through an

avascular region. Using these incident intensity measurements, constants k_1 and k_2 can be calculated:

$$k_1 = \frac{I_{0,549}}{I_{0,560}} \qquad (2.4\text{-}3a)$$

$$k_2 = \frac{I_{0,523}}{I_{0,560}} \qquad (2.4\text{-}3b)$$

Then, (OD_{λ_m} - B) and (OD_{λ_I} - B) from equation 2.2-5 can be calculated by using:

$$OD_{560}\text{-}B = -\log I_{560} - \frac{[\rho \log(\frac{k_2}{I_{523}}) - \log(\frac{k_1}{I_{549}})]}{(\rho - 1)} \qquad (2.4\text{-}4a)$$

$$OD_{549}\text{-}B = \log(\frac{k_1}{I_{549}}) - \frac{[\rho \log(\frac{k_2}{I_{523}}) - \log(\frac{k_1}{I_{549}})]}{(\rho - 1)} \qquad (2.4\text{-}4b)$$

where I_{560}= transmitted intensity at 560 nm

I_{549}= transmitted intensity at 549 nm

I_{523}= transmitted intensity at 523 nm

Finally, oxygen saturation can be calculated using the linear

constants m and b previously determined from the hemoglobin solution experimentation:

$$SO_2 = m\left(\frac{OD_{560} - B}{OD_{549} - B}\right) + b \qquad (2.2\text{-}5)$$

2.5 Conclusions

The above is a brief description of the theoretical basis for the determination of oxygen saturation using photometric methods. Reference (5) should be consulted for a detailed description.

The accuracy of the calculations depends solely upon the accuracy of the incident and transmitted intensity measurements. It is for this reason that a new system, using an optical triplicator, was developed. The following chapters describe the system and the techniques used to perform the necessary measurements.

3.0 OPTICAL TRIPLICATOR

3.1 Introduction

Determining the diffusive flow of oxygen by the three wavelength photometric method of Pittman and Duling (5) requires assuming red blood cells, (hence, [Hb]), and oxygen are uniformly distributed across the vessel. To reduce these inaccurate assumptions, lateral profiles of [Hb] and SO_2 needed to be obtained.

To obtain the lateral profiles, a full cross section of a vessel filtered at each of the three wavelengths needed to be analyzed. Therefore, an optical triplicator was designed to make three copies of the microscopically magnified image of a blood vessel. The triplicator allows for simultaneous filtering of a single image at the three required wavelengths. This allows another inaccurate assumption, uniform composition of blood with respect to time, inherent in Pittman and Duling's "point" measurement system using fiber optic image conduits to be overcome.

3.2 Optical Triplicator Design

The preliminary design of the triplicator consisted of two cube beam splitters and a front surfaced mirror, (Edmund Scientific) Fig. 1. As the Figure illustrates, light exiting the microscope, with intensity I_o, travelling in the z-direction, was allowed to pass through the first beam splitter. This beam splitter theoretically divided the

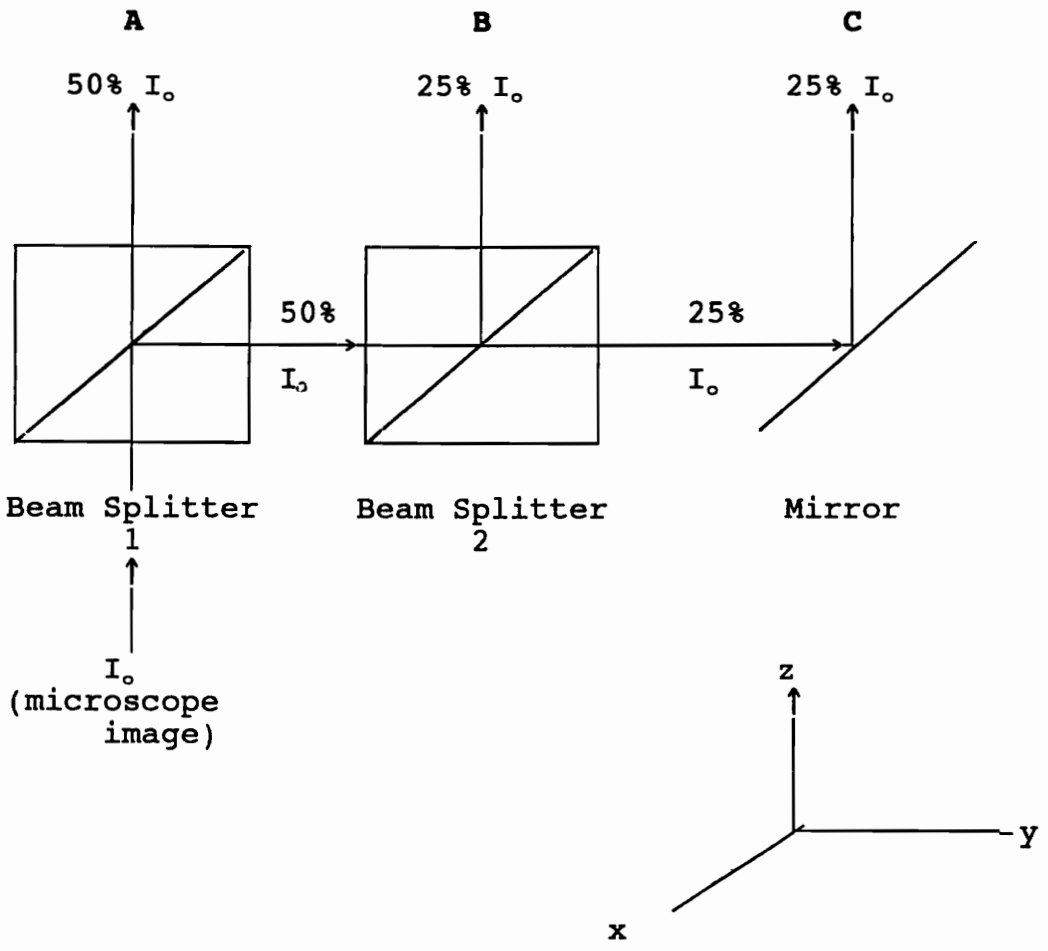

Fig. 1 Preliminary Design of Optical Triplicator

intensity of the light beam in half. A light beam, A, having an intensity 50% of the incident intensity continued in the z-direction, while a second light beam, also having intensity equal to 50% of I_o was directed toward the second beam splitter, in the y-direction. At the second beam splitter, the same deviding operation took place. The light beam having intensity, 50% I_o was divided in half so that a beam B with intensity 25% I_o, exited the beam splitter in the z-direction, parallel to beam A. The other half was directed in the y-direction toward the mirror, which, on contact with the mirror, it was redirected to be parallel with beams A and B.

This design did accomplish the task of triplicating a single image. However, assuring that beams A, B, and C were all parallel could not be accomplished. It was very difficult to keep the mirror perpendicular to the xy-plane while also establishing the necessary 45° angle with respect to the xz-plane. If the mirror was not exactly at the above orientation, beam C would be skewed left to right and/or up and down. With the alignment of the mirror being the overshadowing problem, rethinking the design became necessary.

The new design, Fig. 2, is the current operating design. The alteration consisted of replacing the front surfaced mirror with a right prism, (Edmund Scientific). The beam splitters remained the same, hence, two parallel beams, A and B, were produced. The third beam, C, was generated in the

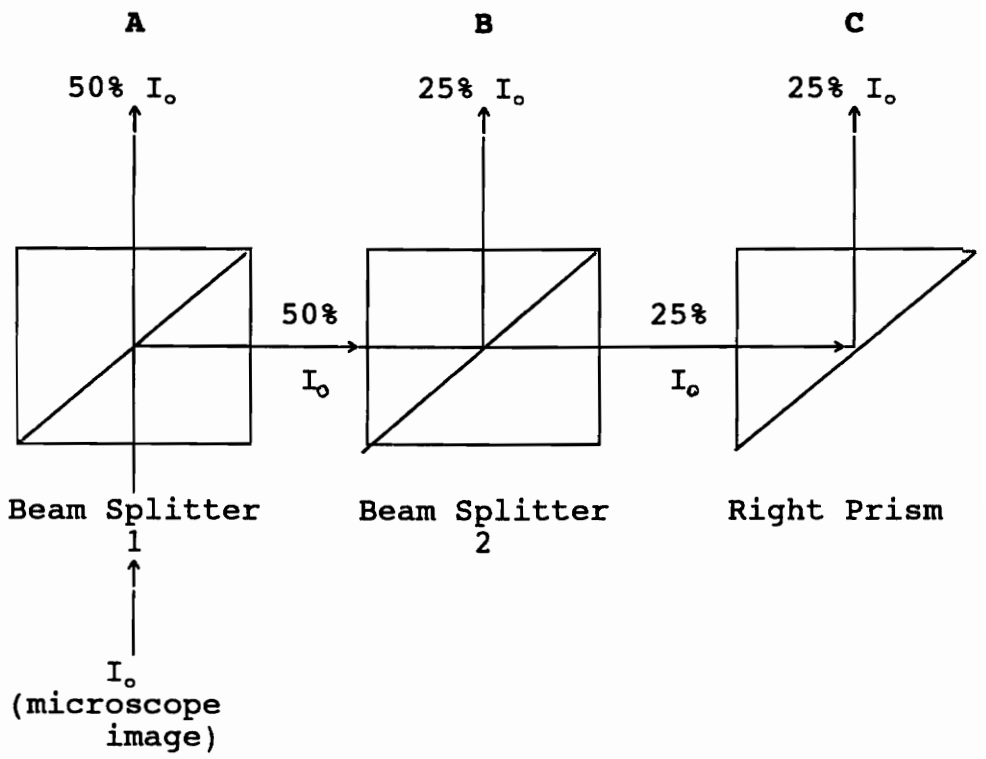

Fig. 2 Operating Design of Optical Triplicator

same manner described above, but, this time using the right prism. The advantage here was that the right prism would sit in the yz-plane (hence, be perpendicular to it) and could more easily be positioned in the 45° orientation.

3.3 Beamsplitters and Prisms

The dividing operation of the beam splitters described above occurs by a mechanism of frustrated total internal reflection (FTIR). FTIR occurs in a gap having a lower index of refraction material, or "frustrating" material, than its surroundings. For example, if the hypotenuse of each of two right prisms was made planar and parallel, to eachother an air gap would be evident. The right prisms could be positioned, by adjusting the gap, to transmit and reflect any portion of the incident beam, therefore producing a beam splitter. The cube type beam splitters used in the operating design are made using a thin, low-index transparent film as the frustrating material. The material of preference would be a low loss reflector so that the absorption loss to the material is very littl. Therefore, the transmission and reflection approach 50% of the incident intensity.

The mechanism of operation for the right prism is similar to that of the beamsplitter, total internal reflection. The light enters the glass prism and on contact with the angled surface undergoes total reflection in a direction 90° from the incident light.

The orientation of the image as it passed through the beamsplitters and the right prisms was of some concern. The concern lay in the need for all three images, A, B, and C to be of the same orientation. As can be seen in Fig. 3, the orientation is preserved. At each reflective surface, the image being reflected is rotated 90°. In contrast, the image travelling through the entire cube does not have its orientation altered.

3.4 Interference Filters

In order to obtain three images each at a single but different wavelength, three filters needed to be used. The type of filter chosen was a bandpass interference filter (Omega Optical Inc.). An interference filter operates on the principles of destructive and constructive interference. Destructive interference occurs when half of superimposing waves exactly cancel the other half; with the net result being no observable wave. Constructive interference is exactly opposite, the interfering waves enhance each other with the net result being an observable wave with higher energy. For an interference filter, a thin film coating is designed to selectively induce destructive interference among some wavelengths and constructive interference among other wavelengths. The thin film coatings are produced in a vacuum chamber. The resulting vapor condenses on a substrate (i.e. glass) while the thickness of the layer is controlled by

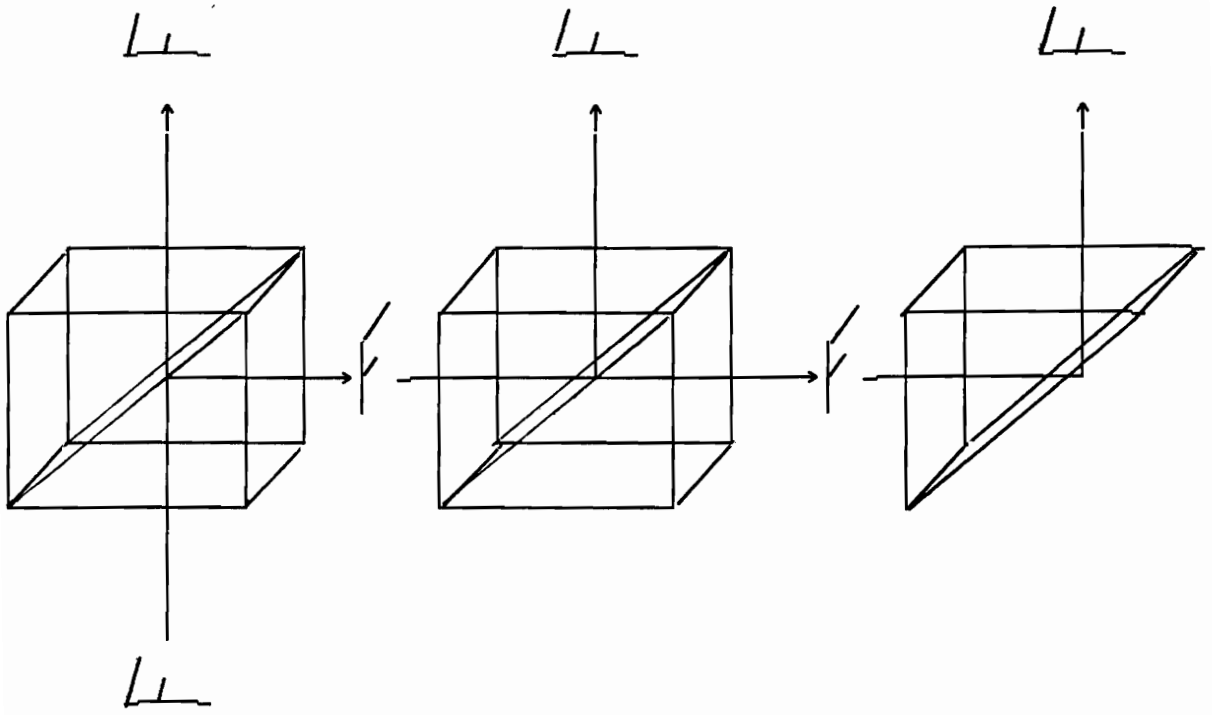

Fig. 3 Orientation of Image Through the System

monitoring the transmission of a monochromatic beam of light passing through the composite. The spectral characteristics can be controlled by the pattern in which the material is allowed to condense, and the actual condensing material used.

A bandpass interference filter is designed by using two quarter-wave reflector stacks, one placed directly upon the other. A quarter-wave reflector stack is composed of alternating layers of dielectric materials each with a different refractive index. Each layer has an optical thickness equivalent to one quarter the principal wavelength, hence the name quarter-wave reflector stack. It is designed to control a central wavelength of light by maximizing the reflection from a coating by destructive interference. Placing two quarter-wave reflector stacks, one on the other, separated by a thin film spacer, as is done for bandpass filters, creates an interferometer that permits transmission of the principal wavelength. Wavelengths other than the principal wavelength will undergo phase differences yielding maximum reflectivity and minimum transmission. Fig. 4 illustrates this function of a bandpass filter, transmitting light at wavelengths around the center wavelength, CWL, and reflecting others. Full width at half maximum, FWHM, which characterizes the width of the pass band; and peak transmission (%T), are controlled by varying the number and arrangement of layers in the stack.

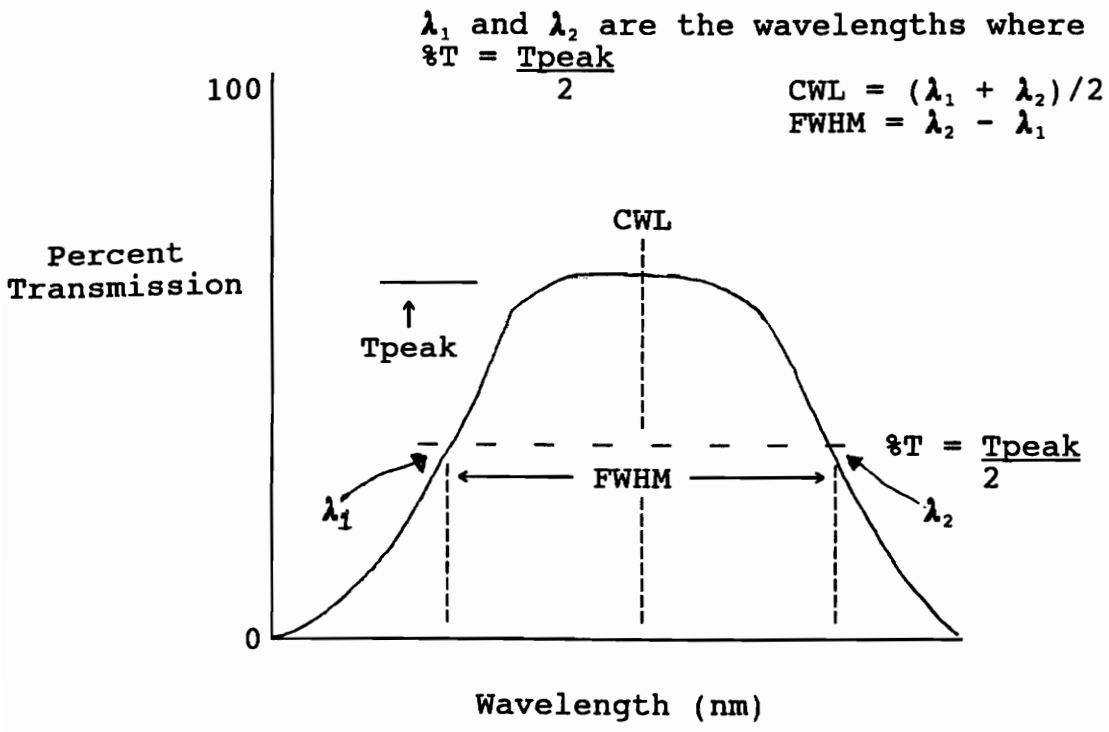

Fig. 4 A Bandpass Filter Spectrum

The optical triplicator required using three bandpass filters each having a different CWL. The CWL's determined for this photometric method were, as previously described, based on the extinction coefficients for oxy- and deoxyhemoglobin. CWL of 560 nm was chosen due to the large difference in oxy- and deoxyhemoglobin extinction coefficients; but, 523 and 549 nm were chosen because the extinction coefficients are equal, or isosbestic. The filters were designed to be narrow bandpass filters. This limits the FWHM to a smaller range, 0.2 nm to 8 nm. Narrow band filters also have a sharp cut-on and cut-off, and they have better blocking outside the pass band. Figs. 5, 6, and 7 illustrate the narrow bandpass filter spectra for CWL's 560, 549, 523 nm, respectively. These graphs are the output from the manufacturer's (Omega) spectrophotometer. The spectral characteristics for each filter are listed in Table 1. As Table 1 shows, the FWHM values are small. These small bandwidths were chosen so not to allow any cross talk between the filters.

The filters were placed in the light path of beams A, B, and C of Fig. 2. The order in which the filters were placed was determined by the intensity of beams A, B, and C; and the attenuation of the image due to each filter. The goal here was to attempt to equalize the intensities reaching the TV camera. If I_o is the incident intensity into the first beam splitter, the intensity of beams A, B, and C

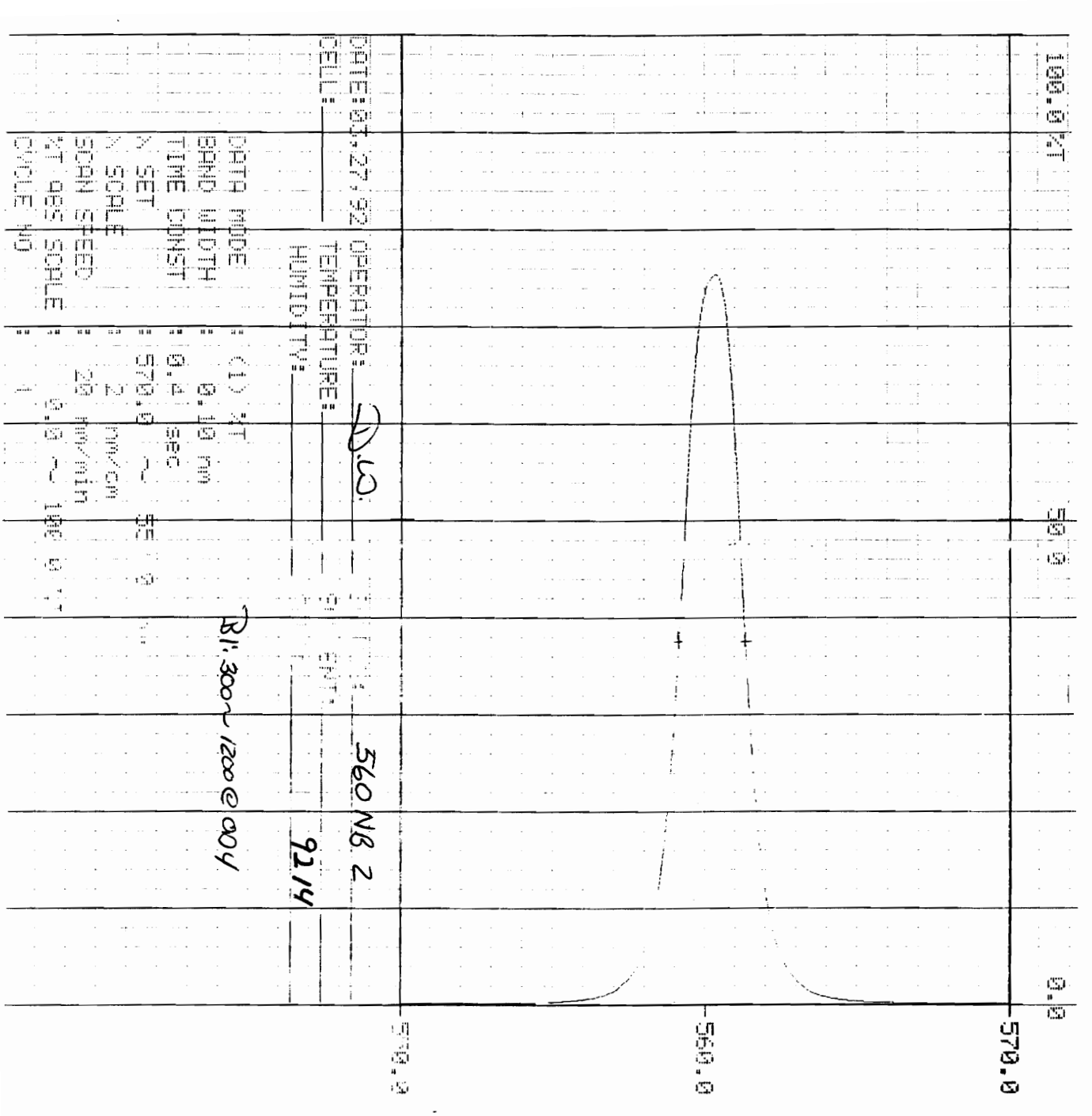

Fig. 5 Spectrophotometer Readout for 560 nm Bandpass Filter (Omega)

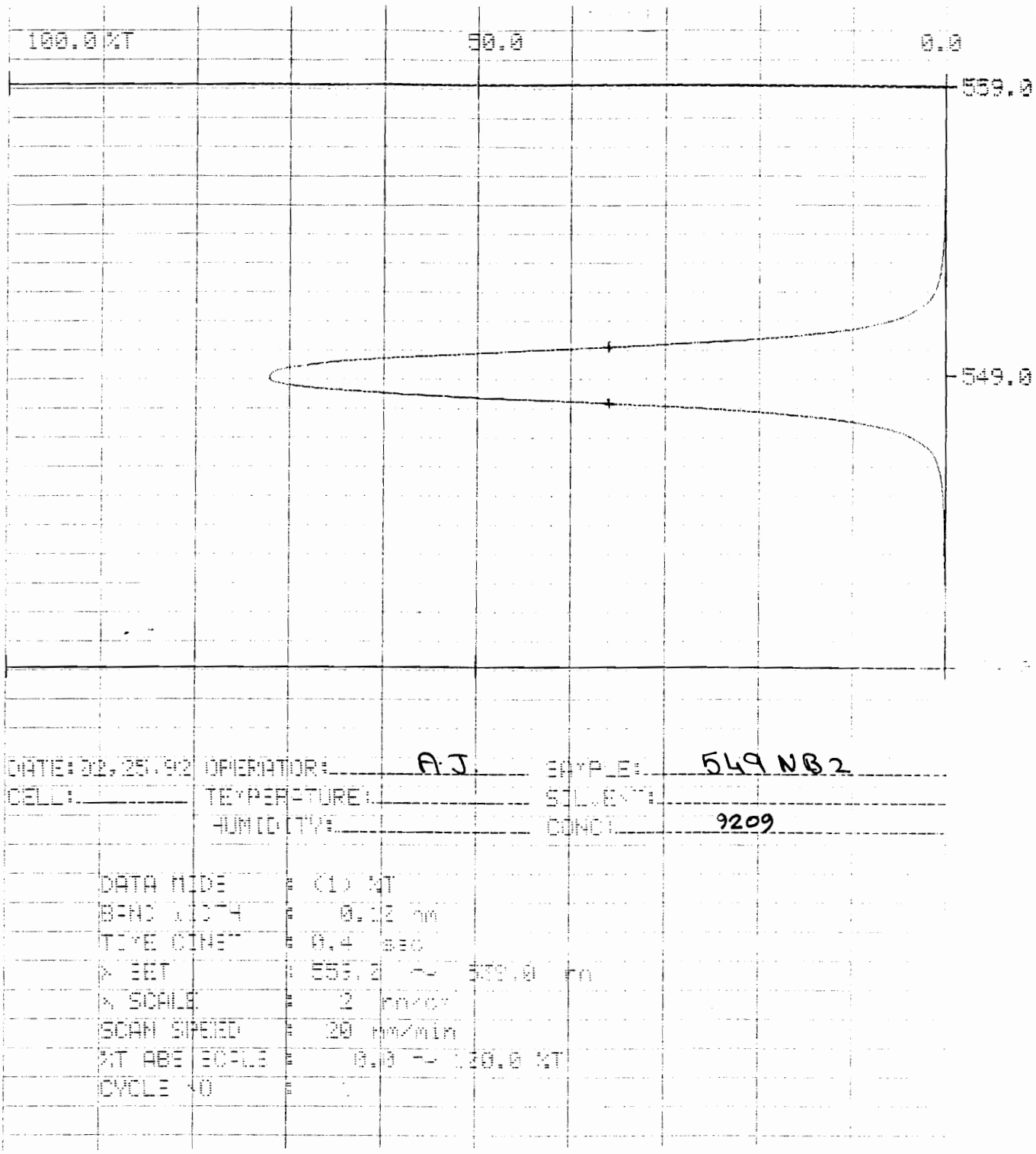

Fig. 6 Spectrophotometer Readout for 549 nm Bandpass Filter (Omega)

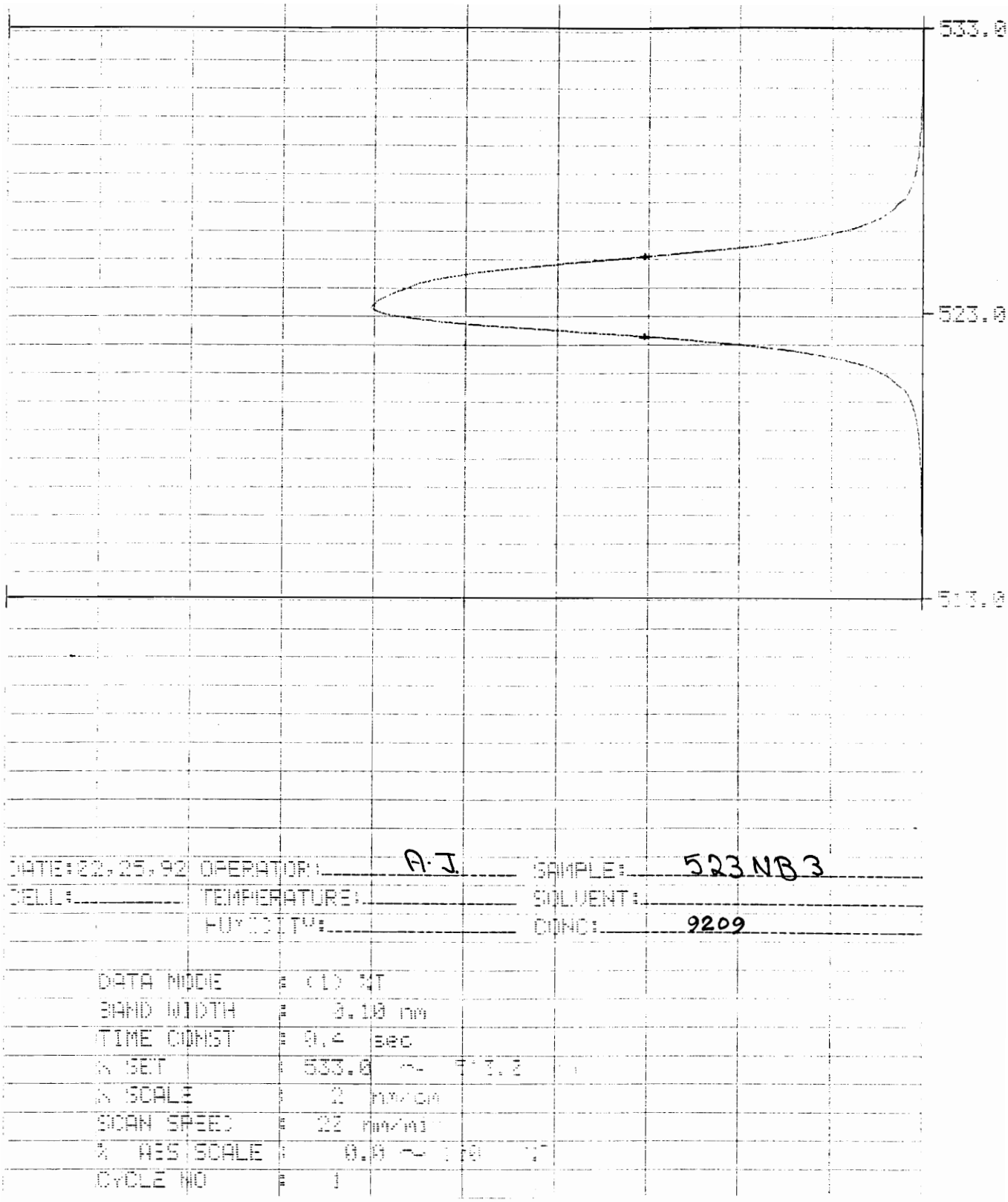

Fig. 7 Spectrophotometer Readout for 523 nm Bandpass Filter (Omega)

Table 1. Spectral Characteristics for Three Bandpass Filters

CWL (nm)	560.2	549.1	523.6
Tpeak (%)	75.2	72.0	60.1
% T	37.6	36.0	30.1
λ_1 (nm)	559.1	548.1	522.1
λ_2 (nm)	561.3	550.1	525.1
FWHM (nm)	2.2	2.0	3.0

are:

$$I_A = 1/2\ f_{\lambda A}\ I_o$$
$$I_B = 1/4\ f_{\lambda B}\ I_o \qquad (3.4\text{-}1)$$
$$I_C = 1/4\ f_{\lambda C}\ I_o$$

where, the constants 1/2, 1/4, and 1/4 are the attenuations due to the beam splitters and the $f_{\lambda A}$, $f_{\lambda B}$, $f_{\lambda C}$ are the attenuations due to the interference filters. It is known that hemoglobin derivatives transmit light better (have a lower extinction coefficient) at 523 nm than at 560 and 549 nm. Also, for the TV camera used in the set-up, (Dage/MTI Model 66 SIT) the spectral sensitivity is greater at 523 nm, with 549 and 560 nm following respectively. It was for these reasons, that the 523 nm filter was placed in the path of light beam C. Since there is little difference between the extinction coefficients for the Hb derivatives at 549 and 560 nm, the spectral sensitivity data was followed. Hence, the 549 nm filter was placed in the path of beam B and the 560 nm filter was placed in the path of beam A. Therefore, equations (3.4-1) can now be represented as:

$$I_A = 1/2\ f_{560}\ I_o$$
$$I_B = 1/4\ f_{549}\ I_o \qquad (3.4\text{-}2)$$
$$I_C = 1/4\ f_{523}\ I_o$$

Intensities I_A, I_B, and I_C should therefore have a smaller range than in the case before, where no interference filters were present.

3.5 Redirection of Tiplicated Images

At this point, the microscopic image had been triplicated and filtered so that each image is monochromatic. The next step was to position the images onto the active area of the TV camera. The active area of the Dage/MTI camera used measured 12.7 mm x 9.53 mm, and the size of beams A, B, and C were all approximately 15 mm in diameter. Therefore, each beam had to be stopped down, by rectangular slits, in order to fit all onto the active area. The distance from the exiting edge of the slits to the active area was designed to be approximately 48 mm. This distance and the size of the active area determined the size of the slit. Three slits measuring 1.5 mm x 7.0 mm, were equally spaced so as to be centered on beams A, B, and C. The light beam exiting the microscope measured 15.1 mm in diameter, and the slits were oriented to section the center region of this beam. This size slit allowed for two rectangular spaces on the active area to be black, with no light contacting them, Fig. 8. The Figure also shows a portion of a 100 μm arteriole; this is the largest diameter vessel expected to be viewed. Using a 50X objective, the arteriole would be 5 mm wide at the exiting point of the microscope. Therefore, the 7 mm slit will allow for the full cross-section of the 100 μm arterial to be imaged.

The final task of the triplicator was to direct the three beams onto the active area of the TV camera. The housing for

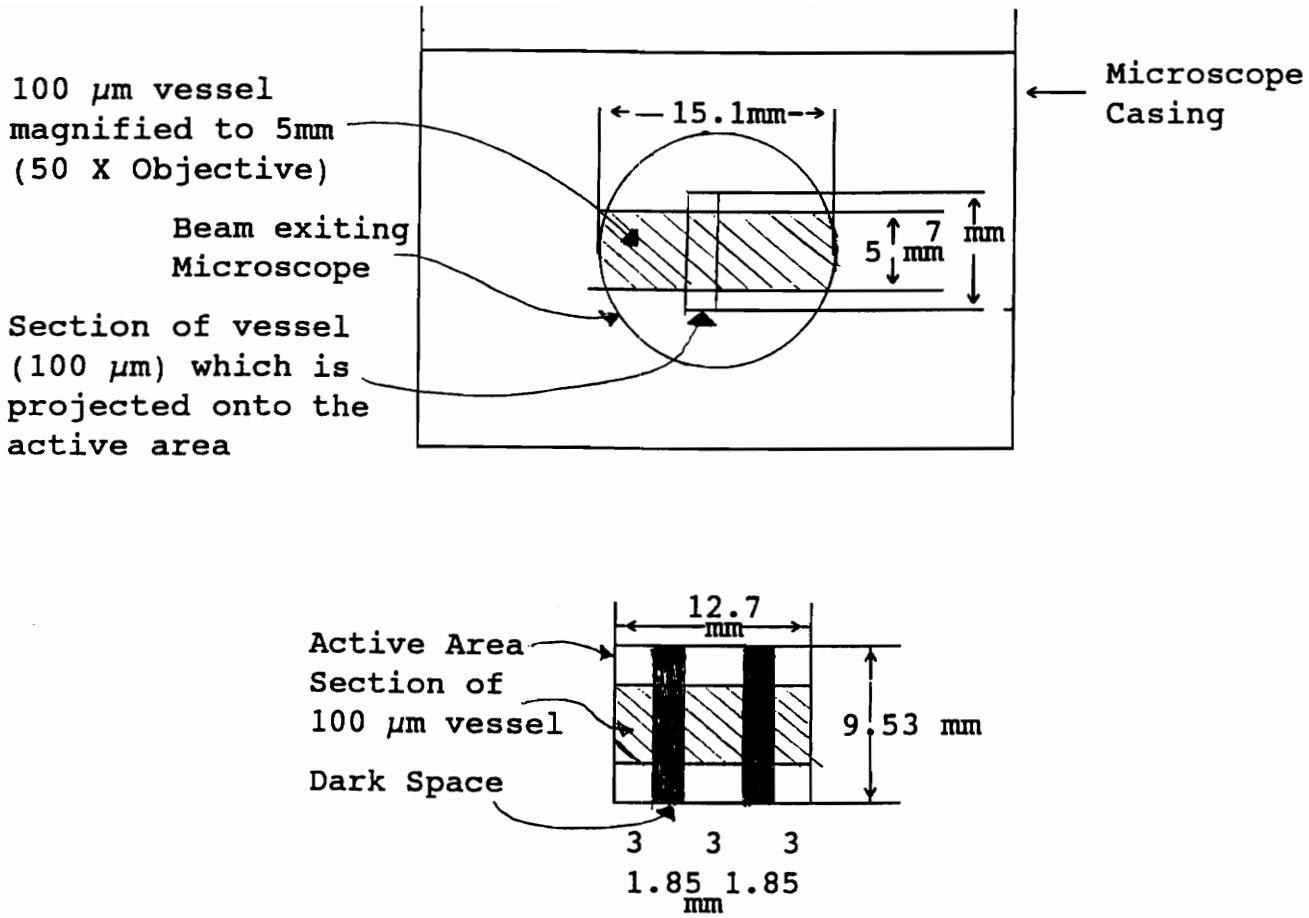

Fig. 8 Dependency of the Slit Size on the Size of the Active Area and the Maximum Size Vessel to be Viewed (100 μm)

the triplicator was designed so that beam C needed no redirection to be in the proper location on the active area. Beams A and B, on the other hand, needed to be translated. This translation was accomplished by again using right prisms (Edmund Scientific). The mechanism for operation is the same as that described previously. As can be seen in Fig. 9, four right prisms were used to translate beams A and B. This Figure also illustrates the optical path of each of the three beams.

3.6 Overall Design Considerations

Several other considerations in the overall set up were taken into account. First, since the light source for the microscope was a xenon; it was necessary to assure that the xenon spectrum contained the three filtering wavelengths (560, 549, and 523 nm). Xenon has a rather broad, flat continuous spectrum over this visible green region (12). Also, xenon arc lamps are high intensity light sources which have a relatively constant intensity over the visible spectrum.

Second, the optical path lengths of the triplicated beams A, B, and C needed be similar. If this wer not the case, the amount of divergence of each beam would be different, hence distorting the image.

Third, since each beam is being stopped down by a single slit, single slit diffraction became a concern. Diffraction occurs when a portion of a wavefront, in this case, a light

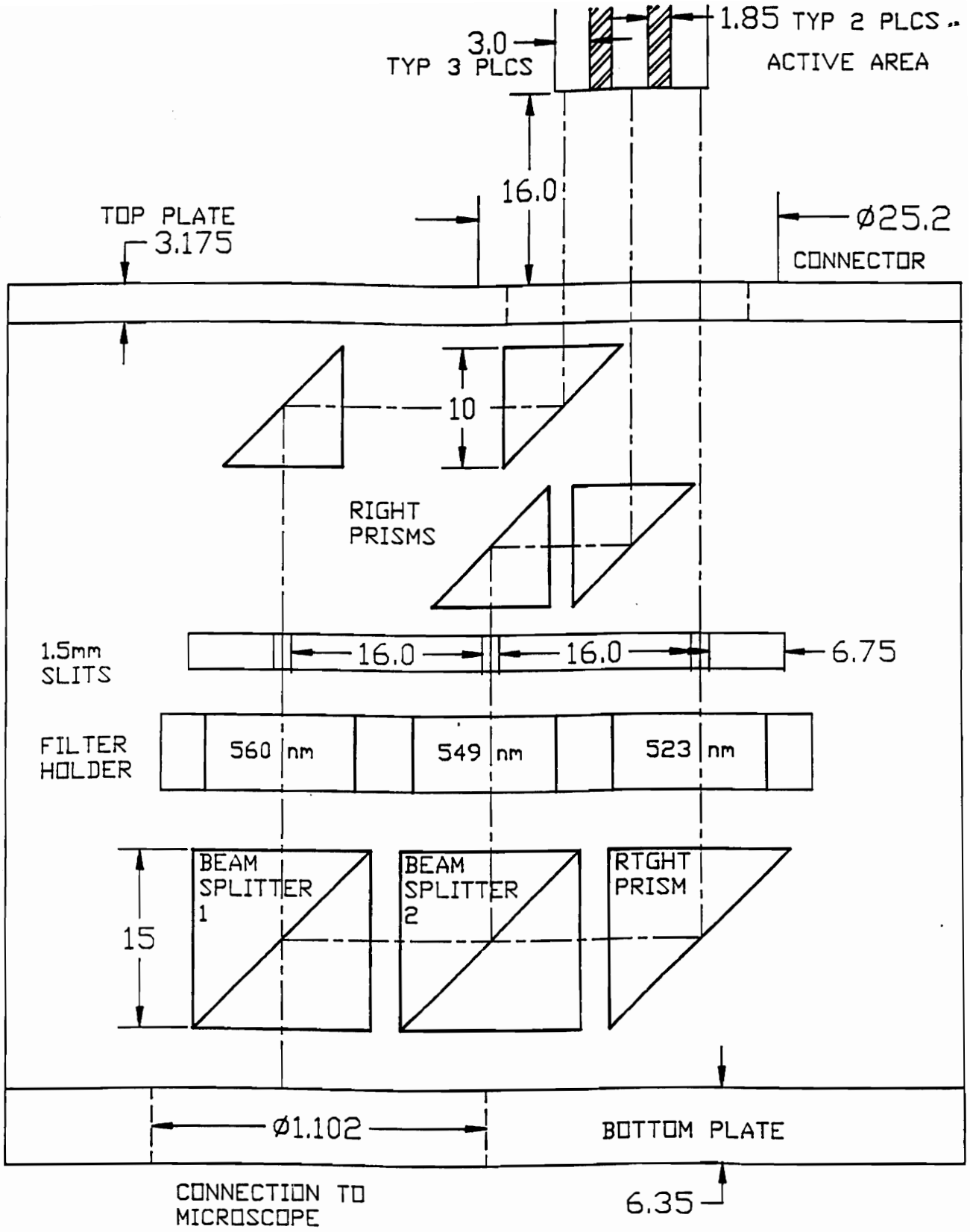

Fig. 9 Optical Triplicator (all dimensions in mm)
(Drawn approximately 2X actual dimension)

wave, is obstructed in some way. The obstruction causes various segments of the wavefront which propagate beyond the obstruction to interfere, producing a representative energy-density distribution referred to as the diffraction pattern. Fraunhofer diffraction, or far field diffraction, of a single slit typically occurs with a slit width of several hundred wavelengths and a length of a few centimeters. A single slit Fraunhofer diffraction pattern is illustrated in Fig. 10. At the ends of the diffraction pattern the intensity is decreased. Although this diffraction pattern was observed when a white viewing screen was placed at the location of the TV camera, in operation, no pattern appeared on the monitor.

The fourth concern, polarization, was recognized after the triplicator was completely assembled. Interference colors appeared just after the beams left their respective optical element (beam splitter or prism). These interference colors were the result of retardation which occurred when the unpolarized light from the xenon arc lamp was partially polarized by the optical elements. To determine that this effect was actually polarization, a polarizer was placed in the path of the unpolarized xenon light. Upon rotation the interference colors changed, indicating the retardation phenomenon. The concern lay with the fact that the 560, 549, and 523 nm wavelengths were selectively absorbed prior to reaching the filters. However, when the filters were put in

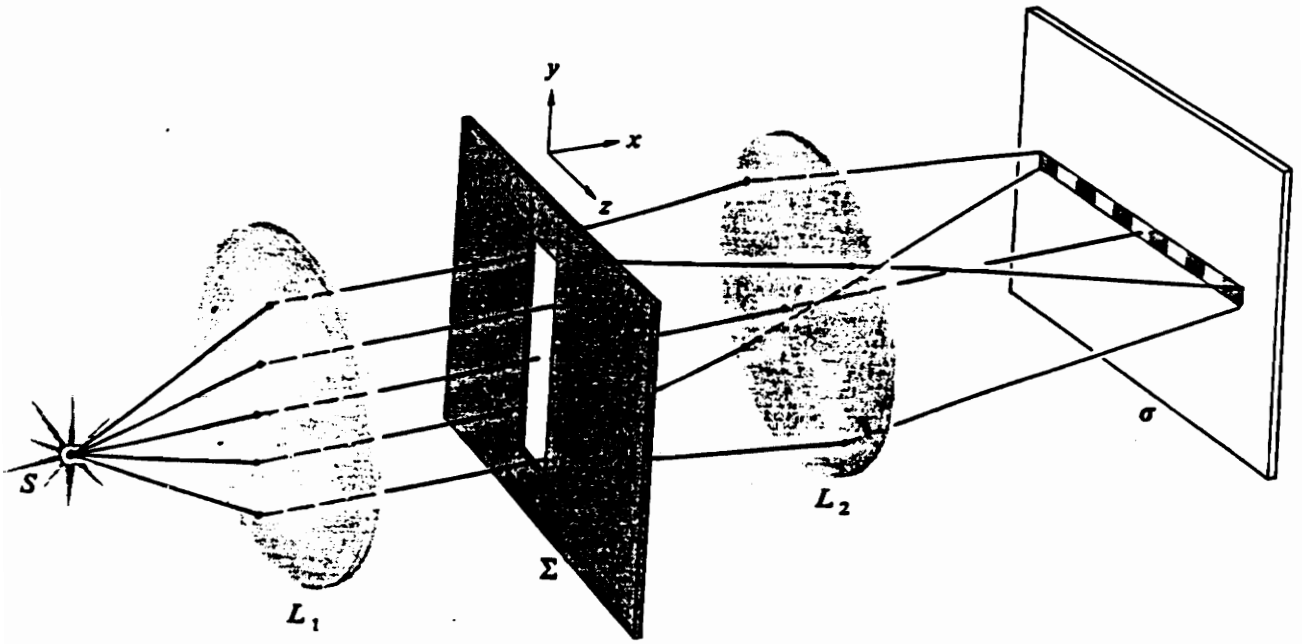

Fig. 10 (a) Single-slit Fraunhofer Diffraction (Hecht)

their locations, monochromatic beams were viewed on the monitor. This indicated that selective absorption did not occur at these particular wavelengths.

Resolution degradation, the fifth design consideration, was realized. It was observed that the 523 nm monochromatic image was not as intense, but "sharper" than were the images from the 560 and 549 nm filters. Resolving power, the minimum distance between two object points that can be resolved in the image, can be represented as:

$$RP = \frac{D}{(1.22\ f\ \lambda)} \qquad (3.6\text{-}1)$$

where, RP = resolving power

D = aperture diameter

f = focal length

λ = wavelength

Therefore, resolving power increases (i.e. the smallest resolvable separation between object points is reduced) for the smaller wavelengths. Although this phenomenon was observed, it did not significantly affect the operation of the triplicator.

3.7 Design Conclusions

The current operating design illustrated in Fig. 2 uses: two beamsplitters and a right prism to triplicate the beam, bandpass filters to obtain monochromatic beams, rectangular

slits to stop the beam size down, and four right prisms to redirect beams B and C toward the active area of the TV camera. This design was constructed in the laboratory to demonstrate the ability of the optical elements to obtain three monochromatic triplicated images. The demonstration was a success. Therefore, a triplicator suitable for the modified design of Pittman and Duling (5) was fabricated.

4.0 FABRICATION OF THE OPTICAL TRIPLICATOR

4.1 Introduction

In an attempt to achieve a triplicated, high quality image on a monitor, an apparatus to mount the optical elements was designed. This housing needed to be located between the microscope and the TV camera. It was also necessary for the apparatus to be level and plumb with respect to the optic axis of the microscope. This would help to ensure that the three images were nearly, if not exactly, the same. Recall, the goal of the triplicator is to take an image from the microscope, triplicate it, direct it into a TV camera, and have, on the monitor, three images in exactly the same orientation.

The following sections will describe the design of the housing, along with the specifications necessary to achieve a high quality triplicated image, and the method in which the optical elements were mounted.

4.2 Design of the Housing for the Optical Triplicator

A box design, Fig. 11, was chosen as the housing for the triplicator. This design was specific to our set up using a Leitz microscope and a Dage/MTI SIT camera. As can be seen in Fig. 11, there is a hole in both the bottom and top plates (plates I and III). The hole in plate I was designed so that the box would fit directly onto the microscope. And, the hole in plate III allowed the box to attach to the camera. A

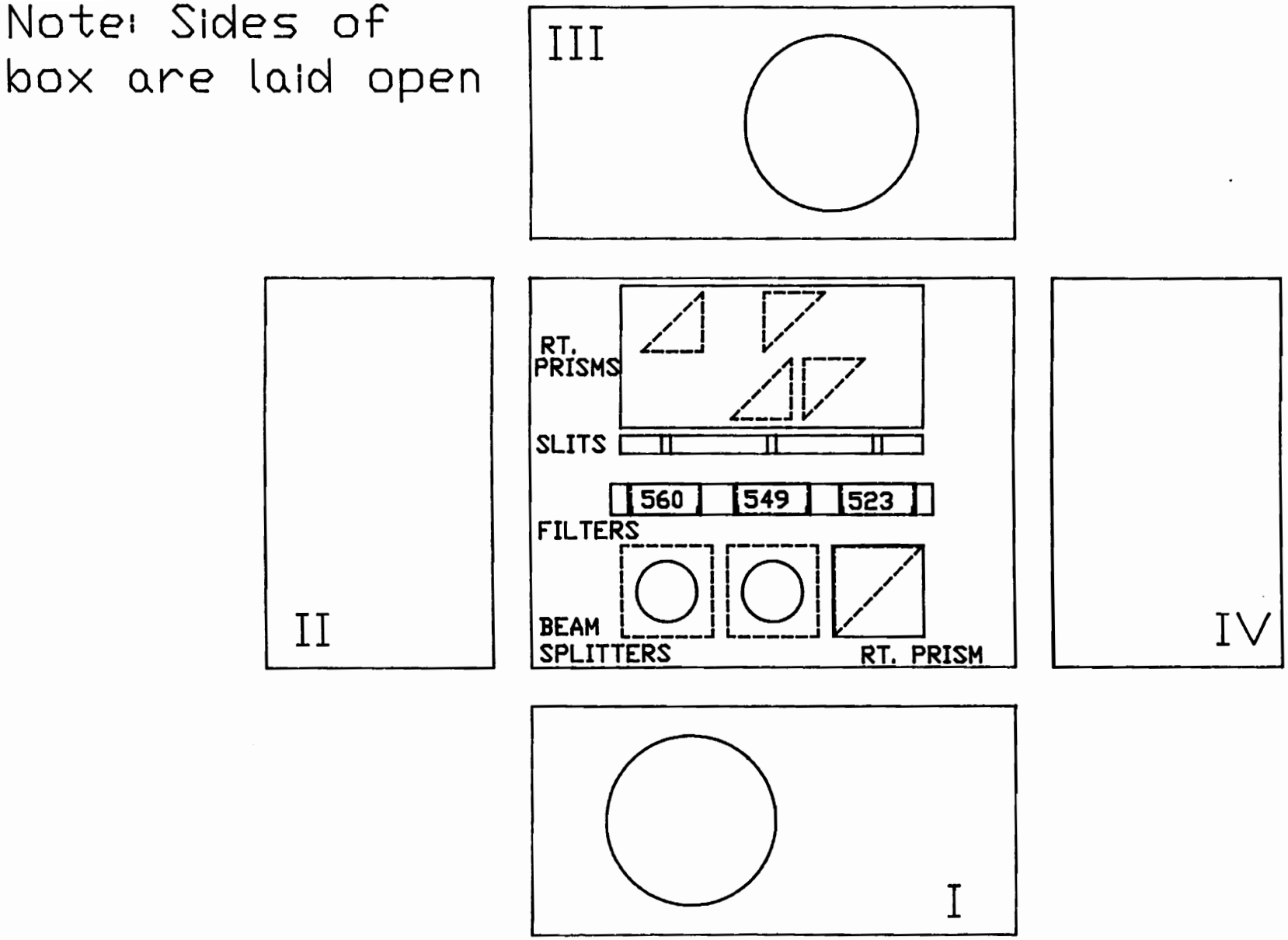

Fig. 11 Housing for Optical Triplicator

threaded cap, which fit into the camera and was previously used to protect the active area of the camera was bored out in the center and adhesively bonded to this hole. This allowed the box to be "suspended" from the camera, Fig. 12. These attachments helped to achieve near complete enclosure of the box. This was desirable to eliminate stray room light from entering into the system. The box was machined using quarter inch plates of aluminum. As Fig. 11 indicates, the overall dimensions of the box were, 92.71 x 73.63 x 76.81 mm.

Plate V (the back plate), Fig. 11, is the plate in which the optical elements were attached. As the drawing shows, there are posts for the beam splitters and plates for the prisms to rest on. It was necessary for these elements to be raised off the back plate so that the center of the image leaving the microscope could be the section which was triplicated. Also, keeping the elements raised eliminated the possibility of distorting the beam as it travelled through the system. If the beamsplitters and prisms were allowed to rest directly on the back plate, and any divergence of the beams was to occur, the back plate would cause a distortion in the diverging beam would have decreased the image quality.

Directly above the posts and plate used for the two beam splitters and prisms to rest on is an aluminum filter holder. This filter holder was attached to the back plate using pins and a single screw. The holder, Fig. 13, was designed

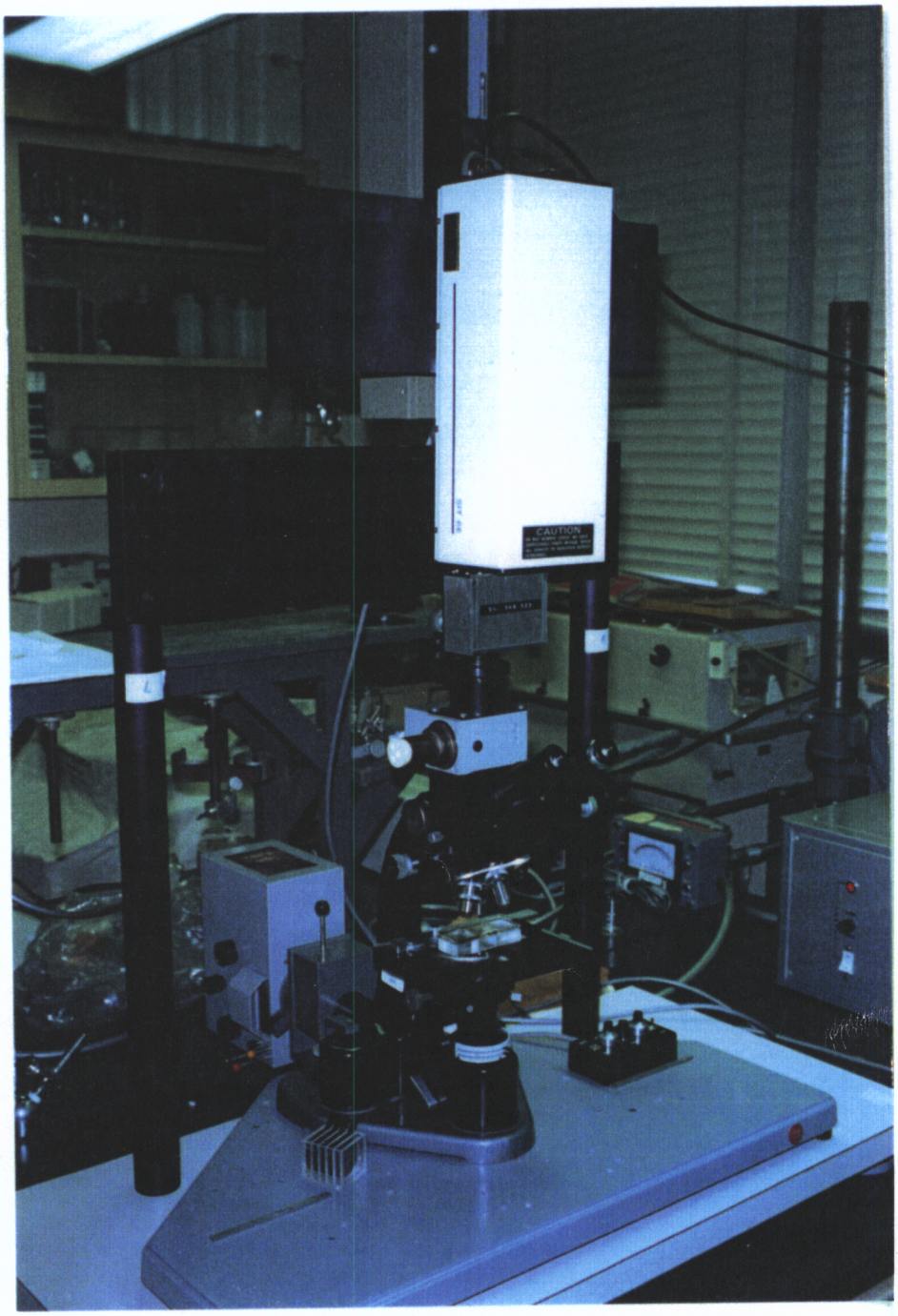

Fig. 12 Optical Triplicator Mounted Between Microscope and Video Camera

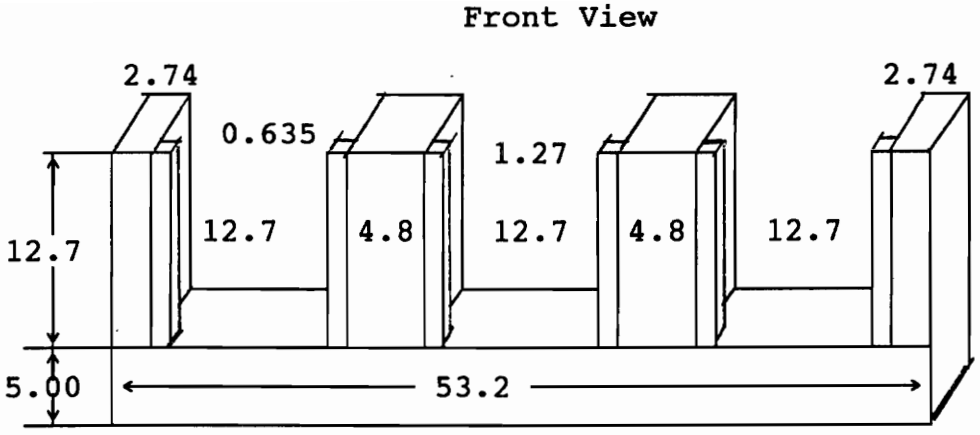

Fig. 13 Interference Filter Holder (all dimensions in mm)
(Drawn approximately 2X actual dimension)

specifically to hold three half-inch square interference filters. It is necessary to ensure that the filters would be perpendicular to the light beam when the triplicator was mounted between the microscope and the camera. Otherwise, tilting the filter may alter the central wavelength being transmitted. Therefore, a lip was machined on the front of the holder. It was also desirable to construct the holder so that the filters could be removed. Hence, the top of the holder was left open.

The slits, Fig. 14, were placed 5 mm from the back edge of the filter holder. In order to make the slits perfectly rectangular, (1.5 mm x 7 mm) spacers were pinned together. Milling holes in a plate would have left undesirable rounded corners. As the figure illustrates, four spacers (A, B, C, D) were pinned together to produce the 1.5 mm width of the slits. Two bars (E and F) were pinned to the top and bottom of the spacers to produce the 7 mm height of the slits. As discussed in section 3.5, these slits were equally spaced in order to section the exact same region of each of the three beams passing through the interference filters.

One final precaution taken to ensure high image quality was to coat the entire inside of the box with flat black (light absorbing, non-scattering) paint. This was to attempt to minimize the amount of light scattered off the walls of the box and, the faces of the filter holder and slits. The

Front View

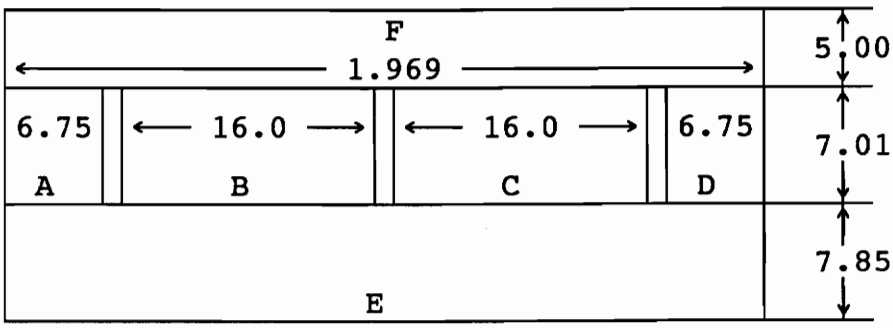

Fig. 14 Slit Design (all dimensions in mm)
(Drawn approximately 2X actual dimension)

scattered light may have entered into the system producing an artifact on the monitor.

4.3 Placement of the Optical Elements

This portion of the fabrication was the most critical and the most difficult. Yet, it was the backbone of the success of the entire experiment. The goal to achieve three identical images on the monitor lay within the accurate placement of the optical elements. The first hurdle to overcome was the type of adhesive to use in order to produce a strong glass to metal seal between the elements and the aluminum box. The adhesive needed to be one that allowed time before curing for maneuverability of the element. The adhesive used was UV Optical Adhesive #61 produced by Norland Optical. A small amount of the glue was applied to the element and it was mounted on its respective post or plate. The glue remained slightly tacky for easy maneuverability until a UV light ray gun was shown on the glue to cure it. The UV rays must, in some way, come directly in contact with the glue, (i.e., an opaque object will not adhere to another opaque object). Hence, any metal to metal seal necessary was accomplished by using "super glue."

Following several methods to align the elements, such as: using a laser beam, using a glass slide with a "+" drawn on it, and even relying on a piece of dust on a microscope slide, it was found that using a stage micrometer was the most

reliable and accurate. Placement was found to be the easiest when the triplicator was mounted between the microscope and the camera. It was also helpful to remove plate III, Fig. 11, from the box and the TV camera so that the light was allowed to travel a long distance. If parallax (i.e., divergence of parallel light rays, hugging the central axis) was achieved within the region defined by the active area, at a long distance, then parallax would be present at the active area of the camera. This method was therefore used to obtain approximate positioning. Then, plate III was replaced and the camera was moved back into position. The stage micrometer was placed on the microscope stage and brought into focus. The triplicated image could be viewed on the monitor. The beamsplitters and prisms were then adjusted so the graduations on the micrometer lay in the same location in each of the three images. This was accomplished using a 20X objective and a 2 mm micrometer with 0.01 mm divisions. After the elements were accurately positioned the UV gun was used to cure the optical adhesive. It was pertinent that a thin film of adhesive was applied to the element to ensure the element would remain level. As Fig. 11 illustrates, the posts for the beamsplitters contained grooves so that excess adhesive would run out the sides when the beamsplitter was mounted.

After the UV adhesive was cured, the system was checked to confirm the orientation and position of the images. Again

the stage micrometer was used and by using the image rotator (Leitz) on the trinocular head of the microscope the image of the micrometer could be rotated a full 360°. This made it possible to view the graduations horizontally and vertically. Using the micrometer it was determined that with a 20X objective, each image is 40 μm wide by 200 μm high on the monitor. To also ensure the orientation of the images, a square grid etched into a microscope slide was viewed. Here, it could be seen how the intersections of the grid lined up with respect to each other.

After repeating the alignment procedure several times, it was determined that image B with respect to image A was translated approximately 20 μm up on the monitor, while image C with respect to image A was translated approximately 20 μm down on the monitor. This was in fact due to the adhesive keeping one or more of the prisms from sitting level. For the application here of viewing blood vessels, a vertical translation was not detrimental. Even if the vessel was translated up or down, the vessel walls would still be prevalent and the image analysis would just need to compensate for this. If however, a horizontal translation was present, this would be detrimental. This would mean that the viewer would not be seeing the exact same image of the vessel. The viewer would be seeing a location either upstream or downstream from the reference image. The final image

confirmation indicated that no horizontal translation was present.

4.4 Fabrication Conclusions

Following several attempts using several different methods to accurately place the optical elements, using the stage micrometer yielded the most precise locations. It is felt that for future work in fabricating an optical triplicator, the method of choice would again be using a stage micrometer. However, an adhesive which had a stronger temporary glass to metal seal than the Norland Optical UV #61 adhesive would be used.

During the installation and calibration preceeding the experimental phase, it was observed that the vertical shift in image B with respect to image A was no longer present. It is thought that this improvement was due to taking more care when performing this final installation. Therefore, the translation error was only a concern when analyzing image C.

5.0 DATA COLLECTION USING VIDEO MICROSCOPY SYSTEM WITH TRIPLICATOR

5.1 Introduction

Upon completion of the design and fabrication of the optical triplicator, modification to the video microscopy system of Duling et. al. (8) was necessary. Fig. 15 illustrates the optical section of the video microscopy system used. The missing portions which will also be described later, is the image analysis system. It was our intent to obtain a video recording of the experiment as it proceeded in order to utilize later the most suitable image analysis software. The entire microscopic field of the triplicated image could be recorded on video tape which allowed multiple areas of the microvessels to be analyzed off-line. Although advantageous, an on-line analysis system was not part of the overall system. The computerized image analysis software allowed for digitizing a single frame of the video recording on regions as small as individual pixels.

Many quantities necessary in the description of microvascular oxygen transport can be obtained using this microscopy system. However, oxygen saturation (SO_2) profiles across arterioles in the hamster retractor muscle were the objective of this first experiment. To accomplish this task, in vitro hemoglobin (Hb) solutions of known oxygen saturations were analyzed. Following this, the actual in vivo

measurements on a hamster retractor muscle were performed.

The following sections will serve as a full description of the entire video microscopy system as well as the procedure for the in vitro and in vivo measurements.

5.2 Video Microscopy System

A block diagram illustrating the optical system and the video system is shown in Fig. 15. The system begins with the xenon lamp attached to a Leitz Laborlux II microscope. The microscope is one of research quality and has excellent optical characteristics for quantitative microscopy. The two outstanding characteristics of this microscope are: the xenon light source, the flat spectra of xenon allows for nearly all the wavelengths in the working range (400 - 600 nm) to be present; and, the condenser lens, which, when adjusted with the pinhole diaphragm, will focus the image of the diaphragm onto the object plane, therefore yielding uniform illumination. The diaphragm also allows the incident beam to be stopped down to a size equal to or less than the object size. This, according to Howling and Fitzgerald (13) is a requirement for accurate spectrophotometry. The objective lenses (10X, 20X, and 50X) have a long working distance and a high numerical aperture; providing good spatial resolution and the ability to collect as much of the transmitted light as possible. The right eyepiece of the microscope contains graduations which allow for approximate vessel diameter

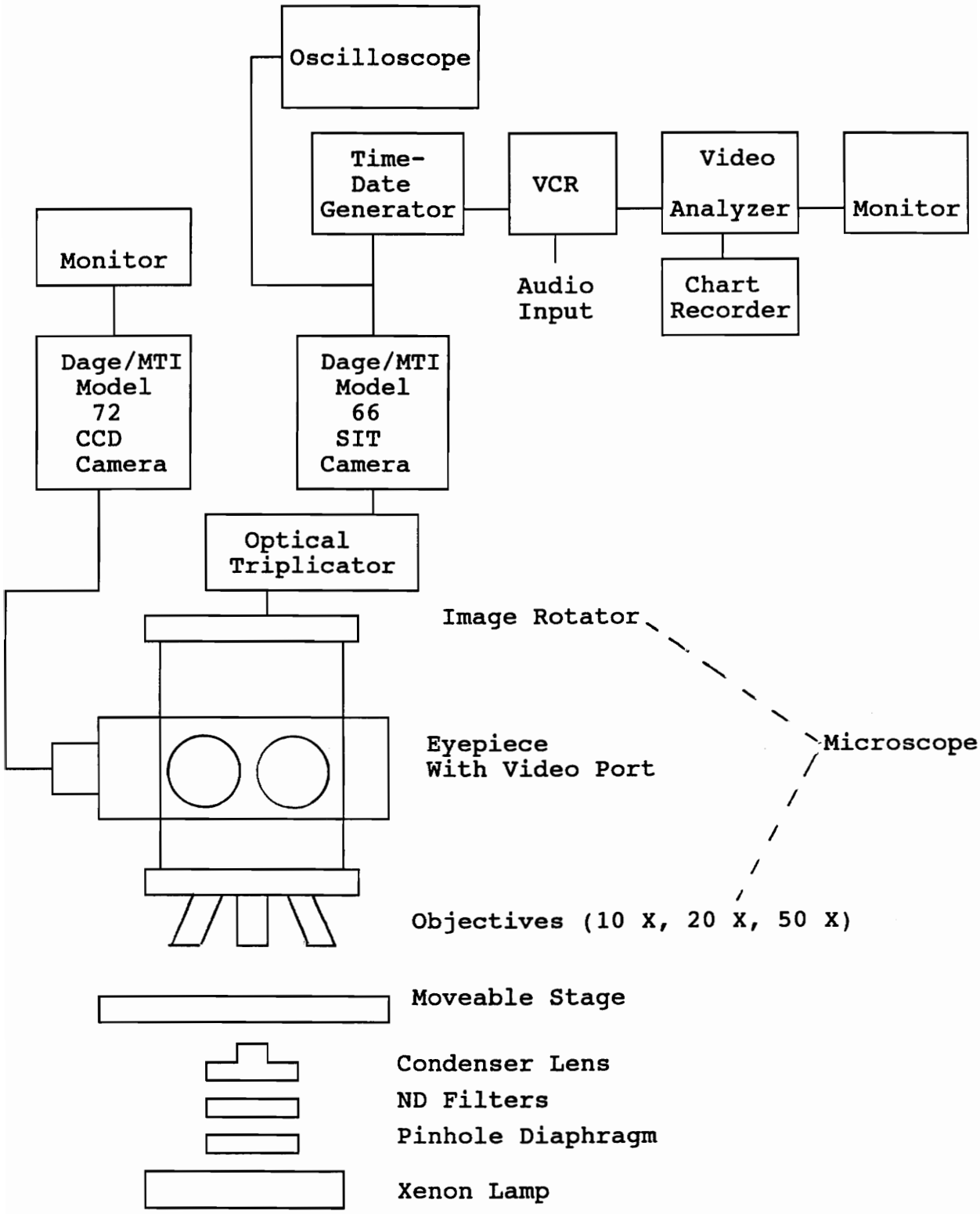

Fig. 15 Optical System and Video System

measurements to be made. Also as part of the eyepiece is a video port in which a CCD camera (Dage/MTI model 72) was attached. The full, non-triplicated, image of the object under study could be viewed on the monitor adjoined to this CCD camera.

As previously discussed, the image rotator on the trinocular head of the microscope allowed for the image of the object under study to be rotated a full 360°. This was advantageous in obtaining on the monitor a horizontal orientation of the vessel.

The image from the microscope then enters the optical triplicator, which as previously described, directs a triplicated image onto the active area of a SIT camera (Dage/MTI model 66). This camera is one which offers low light sensitivity and has a high spectral sensitivity in the working range for this application, 400 - 600 nm wavelengths.

The image from the camera then passes through a time/date generator which superimposes a running time and date on the video recording. Also at this junction, the image is sent into an oscilloscope so that the composite video signal can be monitored (a signal originating from the video camera's sync signal (or its square wave timing pulses) superimposed with the light intensity from the image). Setting this composite signal to yield a 0.7 volt intensity signal above the 0.3 volt sync signal (the 1 volt peak-to-peak composite video signal)

is accomplished by using the KV and gain adjustments on the SIT camera. These adjustments allow for the black level to be optimized.

The image from the time/date generator then travels into the VCR for recording. The VCR is also equipped with an audio input. This proved helpful during the image analysis procedure. The documentation on the video recording simplified the process of determining which section of the microvessel was being triplicated and, other pertinent information could be obtained. Two video input channels on the VCR allowed for the full field of view image from the CCD camera to also be recorded.

After the image passed through the VCR, it entered a video analyzer (Colorado Video 321 Image Analyzer). This video analyzer produced an on-line estimation of the intensity profile. The analyzer generates a pair of cursor lines which when used in the densitometric mode allowed for point measurements to be made. The point at which the vertical and horizontal cursor lines intersect was the measuring point. At this point, an analog output, corresponding to the intensity of the video signal amplitude, was generated and displayed on the left side of the monitor. Using the analyzer in the slow scan mode allowed for the video image to be scanned either along the vertical or horizontal cursor line, also producing an analog output. By placing two horizontal, or vertical,

cursor lines at the edges of the microvessel, diameter measurements were made. A conventional chart recorder was also used as an on-line estimation of the analog output from the video analyzer. A hard copy read out from the chart recorder was reviewed and compared with the data obtained using the image processing software. The final component in the video system is the monitor. The monitor displays the triplicated image originating from the SIT camera along with any data from the video analyzer.

5.3 Image Analysis System

The image analysis system used was based upon the IMAGELAB software produced by Werner Frei Associates (Venice, California). This image processing and analysis software is compatible with IBM AT computers. It can be used to view, evaluate, and measure visual data. As previously discussed, using a video recording was most advantageous in our application.

A block diagram illustrating the image analysis system is shown in Fig. 16. The video output from the VCR enters a Zenith IBM PC computer which contains a frame grabber (VISIONplus Overlay Frame Grabber (OFG)) board attached to the expansion slot. The frame grabber accepts and digitizes the video signal from the VCR, and stores the digitized image data in its memory. The frame grabber also outputs a video signal to the viewing monitor which displays the images being

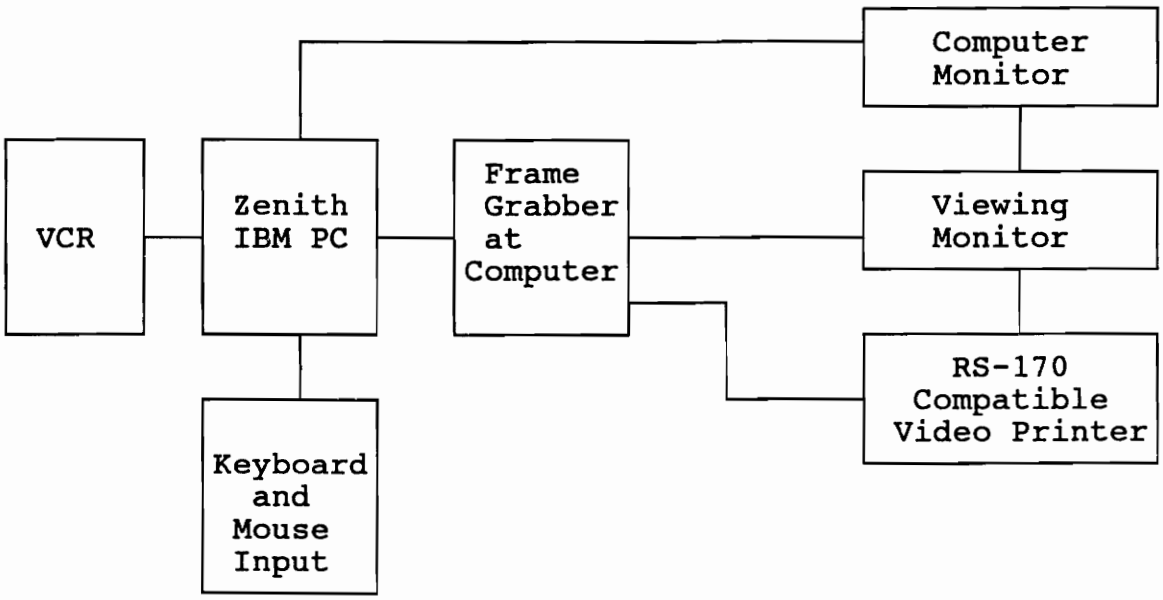

Fig. 16 Image Analysis System

processed. A hard copy of the image being processed and displayed on the viewing monitor can also be obtained by a video printer (RS-170 compatible video printer). The computer operates on a DOS operating system, using keyboard and mouse input data. The computer monitor is used primarily when the system is toggled between DOS and IMAGELAB. Otherwise, all functions are menu driven from the viewing monitor and the mouse.

The analysis process begins by playing back the video recording and capturing a single frame. Once this frame is captured, it is stored in the frame grabber's memory. This frame is then analyzed by digitizing the image. Digitizing can be accomplished either along a line segment or at a single pixel point. Either method yields intensity data (gray scale values) which are relative to the black level. When the line segment method is used, a plot of gray scale values versus position on the line can be generated. An example is shown in Fig. 17. The graph illustrates the low intensity values for the portion of the line segment out of the first triplicated image with the values increasing upon entering the image. This line segment method provided intensity profile information along the line (i.e. across the diameter of a microvessel). However, due to limitations with the software, the data used to generate these plots could not be obtained from the computer. Hence, in order for the SO_2 calculations

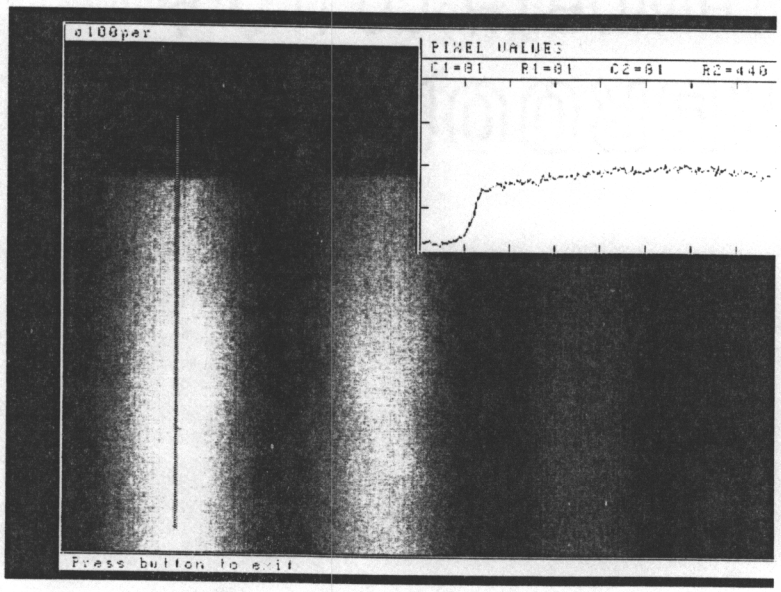

560

Fig. 17 Example of plot generated using IMAGELAB software in the digitizing mode using line segments.

to be performed, pixel intensity values were recorded. Once these pixel values were generated and recorded, statistical analysis was performed on the data before they were used in the calculations for SO_2.

Microvessel diameters could also be obtained using the IMAGELAB software. First, an image from a stage micrometer was captured and stored at each of the three magnifications (10X, 20X, and 50X). Then, a calibration method was performed to obtain a conversion value for converting number of pixels to micrometers at each magnification. Once these conversion factors were calculated, a line segment could be drawn from one edge of the microvessel to the other. The number of pixels traversed could be determined and the approximate diameter calculated.

Many other image processing tools exist with the IMAGELAB software, such as features to filter, zoom and pan, color, contrast, and enhance. Of this limited list, the enhance and zoom and pan features were the only other tools utilized. The enhance feature enabled the walls of the microvessel to be viewed more accurately, therefore increasing the accuracy of the diameter measurements. The zoom and pan feature enlarged the image to show the microvessel regions more explicitly.

The video microscopy and image processing systems described above were utilized in the in vitro and in vivo experiments to be described.

5.4 Experimental System Preparation

Prior to making in vitro and in vivo measurements, the video microscopy system needed to be realigned and calibrated. Again using the stage micrometer, the horizontal and vertical translations were checked. As before, no horizontal translation was noted. However, with respect to image A, image C was translated slightly in the vertical direction. The microslide having a square grid etched on it was also used to assure no rotational inaccuracies were present. As this process was taking place, the images were being recorded to be used later in the analysis procedure. These images would provide the means for determining the extent to which image C was vertically translated with respect to image A.

Next, the gain and kilovolt (KV) settings on the SIT camera were manually adjusted to give a 1 volt peak-to-peak composite video signal on the oscilloscope. It was also noted at this point that neutral density (ND) filters may be needed in the path of the incident light to adjust the overall light level. The ND filters placed between the pinhole diaphragm and the condenser lens, Fig. 15, brought the light intensity into an acceptable range.

The final calibration method performed was checking the linearity response of the SIT camera with the ND filters. Each ND filter was placed in the path of the incident beam while recordings were taken at each of the three wavelengths.

A linear relationship should be present between the intensity data and the percent transmission of the ND filters. A linear relationship eases the analysis procedure when converting analog data into light intensities. Data obtained at 560 nm is listed in Table 2. The corresponding graph in Fig. 18 illustrates the linear relationship of the data. The r-coefficient, indicating how well the data fits a straight line, is 0.994, with 1.000 being a perfect fit. Therefore, it can be assumed from this, and from the data taken at 549 and 523 nm, that the response of the SIT camera is linear.

5.5 Hemoglobin Solution - In Vitro

Deoxy- (0% SO_2) and oxyhemoglobin (100% SO_2, HbO_2) solutions were prepared and analyzed in order to calculate the slope (m) and intercept (b) used in the determination of SO_2:

$$SO_2 = m\frac{(OD_{560} - B)}{(OD_{549} - B)} + b \qquad (5.5\text{-}1)$$

A Hb solution is made by lysing (i.e. breaking the red blood cell membrane) a red blood cell (RBC) suspension. To accomplish this, a blood sample is centrifuged and the plasma and buffy coat are removed. The remaining RBC's are resuspended in a saline solution and washed several times. The cells are then lysed in a known volume of distilled water to produce the desired Hb concentration [Hb]. The mixture

TABLE 2

Linearity of Dage/MTI Model 66 SIT Camera at 560 nm

ND Filters	Relative %T @560 nm	DC Output
10%	100	2.2
10 + 50%	54.7	1.2
10 + 35 %	32.5	0.95
10 + 20%	19.5	0.75
10 + 2%	1.3	0.43
Black	0	0.4

Fig. 18 Linearity of SIT Camera at 560 nm

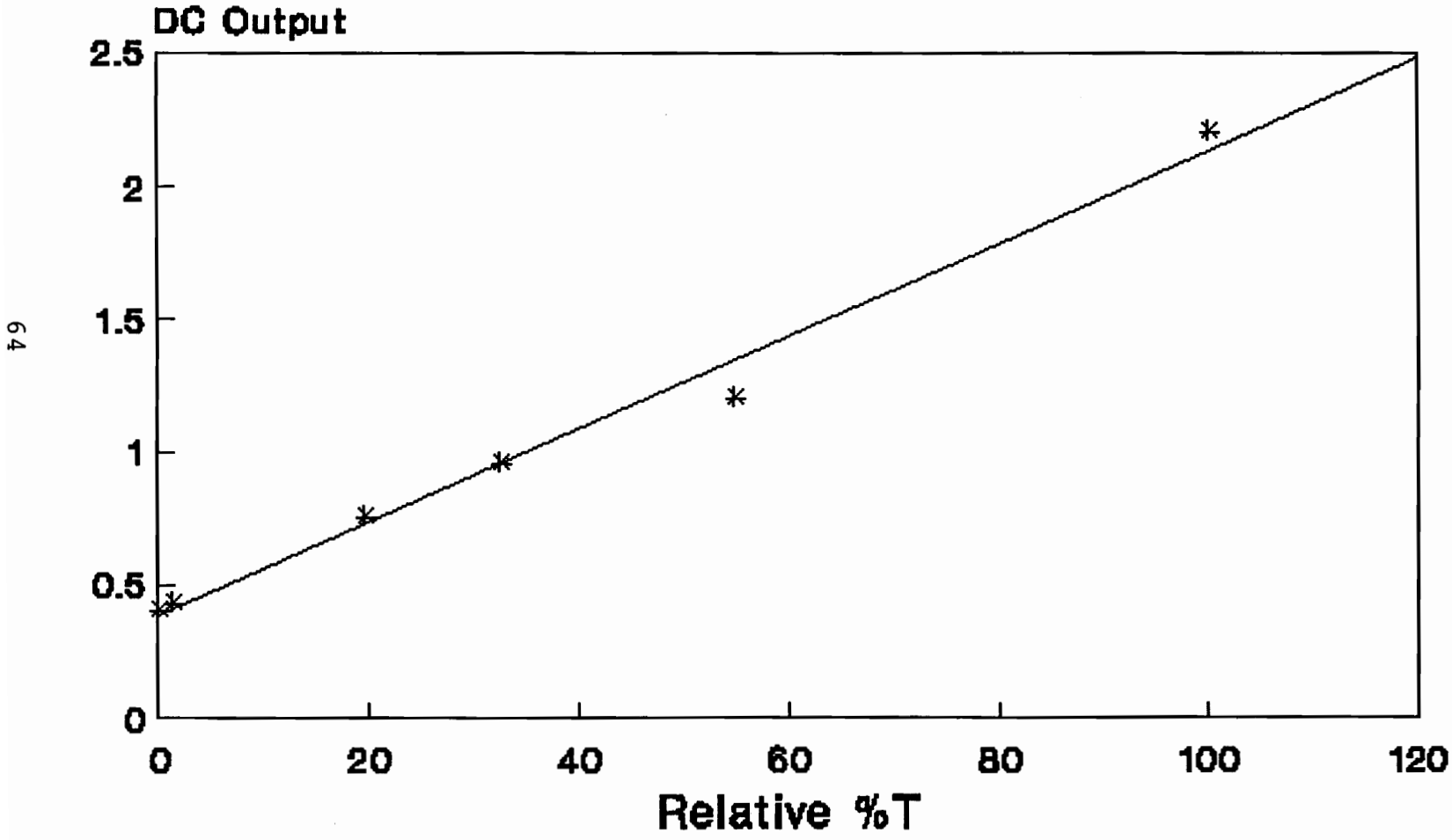

should then be centrifuged in a refrigerated centrifuge at high speeds (15,000 g for 30 minutes). This step removes the cell plasma membranes and other debris. The supernatant will be the Hb solution ready for use in the in vitro studies. It should be cautioned not to allow the Hb solution to be exposed to air.

To make an oxyhemoglobin solution from this supernatant clear Hb solution, a small amount of the Hb solution should be placed in a flask which had previously been flushed with 100% O_2. The solution should be swirled around the flask to assure full oxygenation of the Hb.

A few sodium dithionite crystals are added to a nickel size portion of the Hb solution to prepare a deoxyhemoglobin solution. Within seconds, the sodium dithionite will deoxygenate the Hb completely. This solution should be used immediately so not to allow time for the dithionite to affect the Hb molecule.

To begin the experiment, each of these solutions, deoxy- and oxyhemoglobin, along with a distilled water sample were placed in microslides (Vitro Dynamics Inc.). The microslide is a small glass tube with a rectangular cross-section. A small amount of each was drawn up into a microslide by capillary action. The rectangular cross-section helps to eliminate refraction errors induced when using tubes with a circular cross-section. The microslide used in this

application had a 100 μm cross-section, hence a 100 μm path length. The distilled water sample is used to determine the incident intensity value, Io, in the optical density (OD) equation:

$$OD=\log\left(\frac{I_0}{I}\right) \tag{5.5-2}$$

Measurements are made by placing the three samples on the microscope stage, Fig. 19, and video recording the triplicated image for later analysis. An example of an image captured using IMAGELAB is shown in Fig. 20. This specific example is the triplicated image of an oxyhemoglobin solution at each of the measuring wavelengths (560, 549, and 523 nm). A similar image is captured for both the deoxyhemoglobin solution and the distilled water sample. Recall, that ND filters may be placed on the pinhole diaphragm to attenuate the incident intensity, so not to saturate the SIT camera.

Using IMAGELAB, each sample at each of the three wavelengths was digitized and the data recorded. Caution was taken to digitize along the centerline of the image so not to involve the edges of the microslide. These data proved useful in: first, assuring the necessary isosbesticity of the 549 and 523 nm filters; second, the optical density ratio between the 549 and 523 nm filters could be calculated:

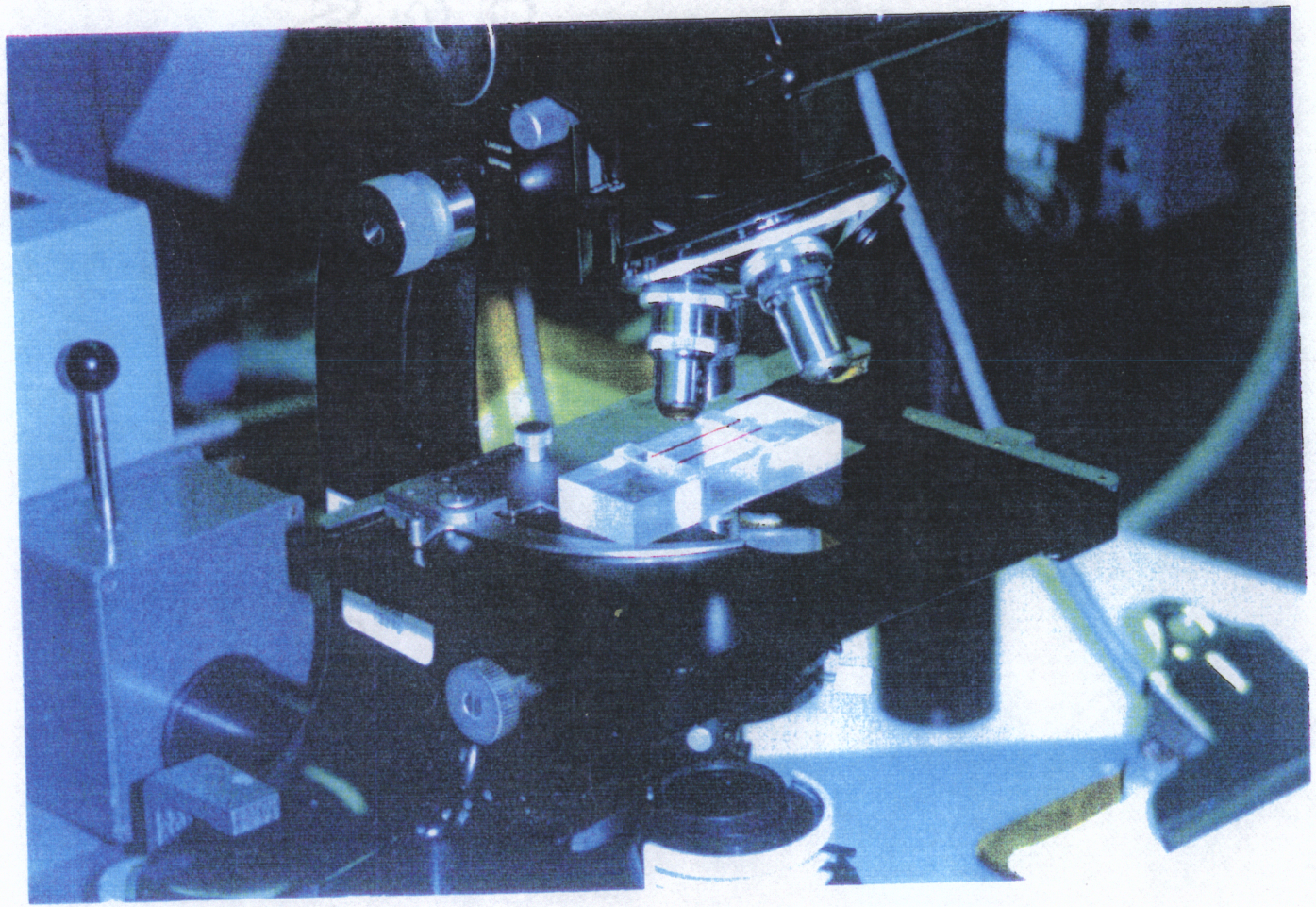

Fig. 19 Three Microslide Hemoglobin Solutions on the Microscope Stage

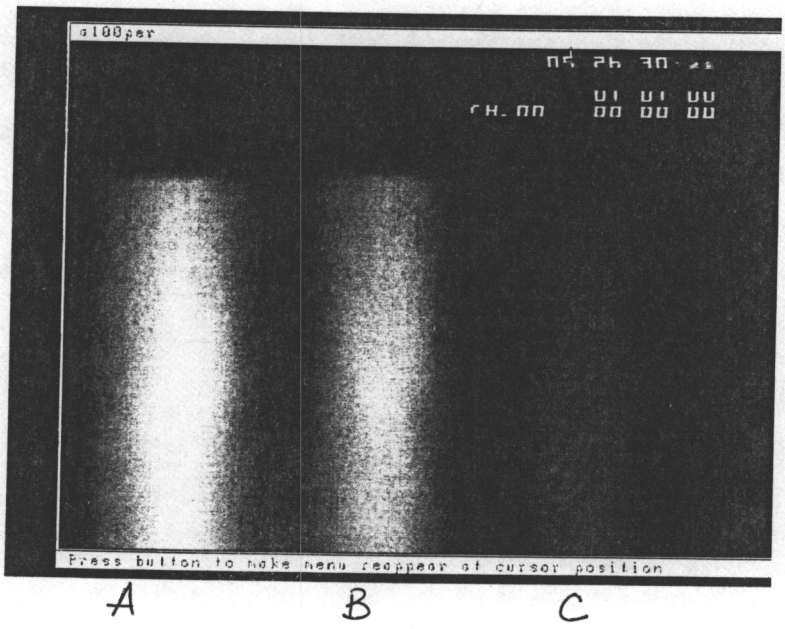

Fig. 20 Triplicated image of a oxyhemoglobin solution at A = 560 nm B = 549 nm and C = 523 nm

$$\rho = \left(\frac{OD_{549}}{OD_{523}}\right)$$

(5.5-3)

Recall, this value is used in the calculation of the scattering term B:

$$B = \frac{(\rho OD_{523} - OD_{549})}{(\rho - 1)}$$

(5.5-4)

And, as discussed previously, the slope and intercept of the SO_2 relationship (5.5-1) can be calculated by using:

$$m = \frac{1}{(R_1 - R_0)}$$

$$b = -\frac{R_0}{(R_1 - R_0)}$$

(5.5-5)

where $R_1 = OD_{560}/OD_{523}$ for the oxyhemoglobin solution and $R_0 = OD_{560}/OD_{523}$ for the deoxyhemoglobin solution.

After acquiring these constants, an in vivo measurement could be made using the hamster retractor muscle.

5.6 In Vivo Measurements

The ambition for performing in vivo measurements was to determine the SO_2 profile across an arteriole, and to observe how this profile changed at a bifurcation.

In vivo measurements can be made using the hamster

retractor muscle. Preparation of the muscle is described by Sullivan and Pittman (14). Once the muscle is exposed, it is covered with a transparent, gas impermeable covering (Saran Wrap works well). This retards the drying of the retractor muscle. The hamster is placed on a plexiglass stage, which has a continuous flow of warm water through it to keep the hamster warm, Fig. 21. The hamster also experiences a continuous infusion of anesthetic.

Choosing a small hamster (70-80g) will optimize the in vivo technique. A smaller hamster will not have developed a large amount of connective tissue around the retractor muscle. Thus, the optical clarity of a superficial arteriole in a thin section of the muscle will be improved.

Once the hamster is situated on the stage, the retractor muscle is searched for a 40 - 50 μm diameter arteriole having a long branch. This is accomplished by using either the 10X or 20X objective. A video recording is taken of the region for the subsequent analysis. The 50X objective is used for the actual measurements along the arteriole. Triplicated images are recorded at several measurement sites along the arteriole near a bifurcation, Fig. 22. The figure shows four measurement sites.

One unavoidable hindrance with in vivo measurements is the problem of not having a direct estimate of light intensity incident upon the arteriole. This value, Io, is, as was in

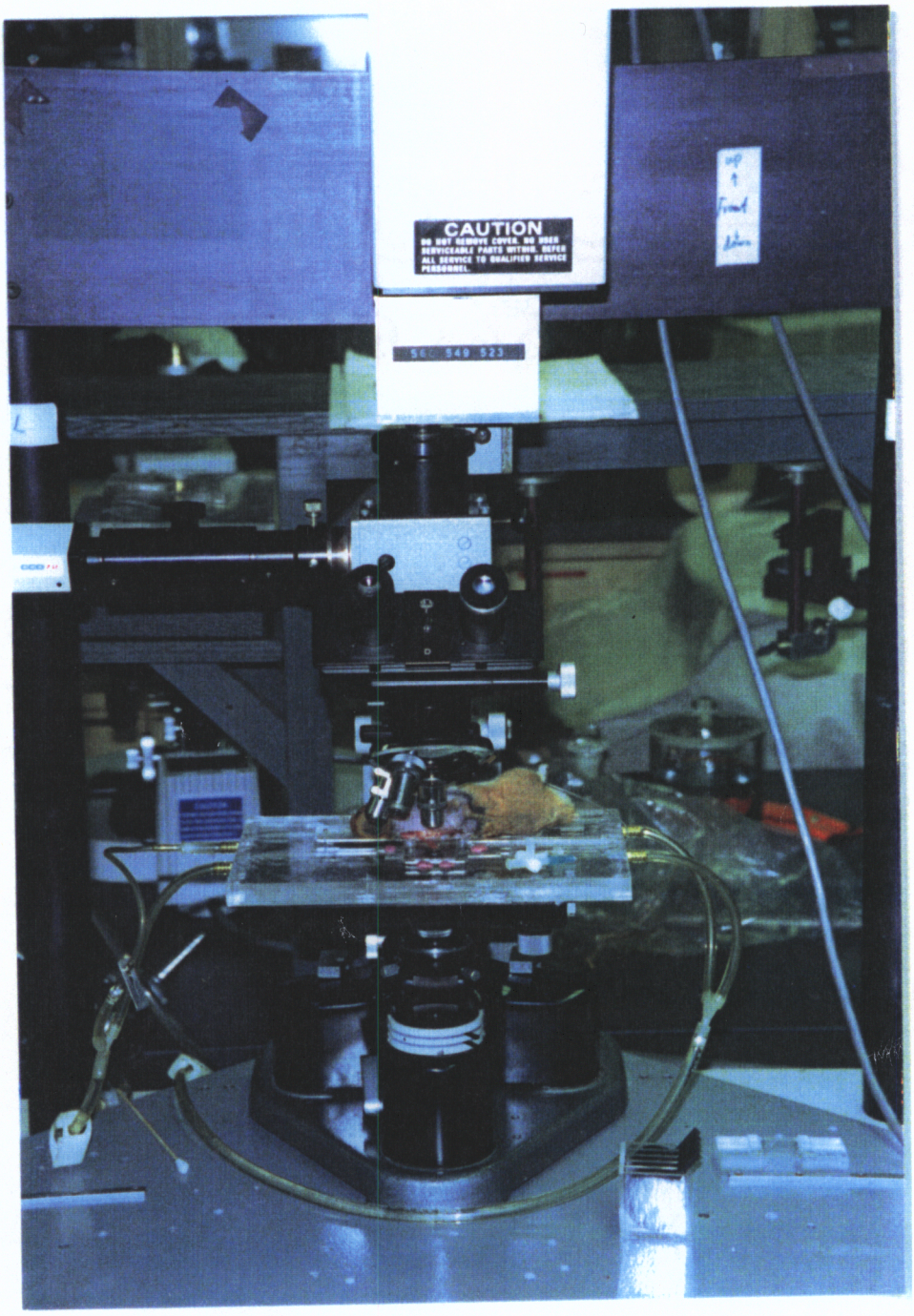

Fig. 21 Hamster Positioned on the Microscopes Stage

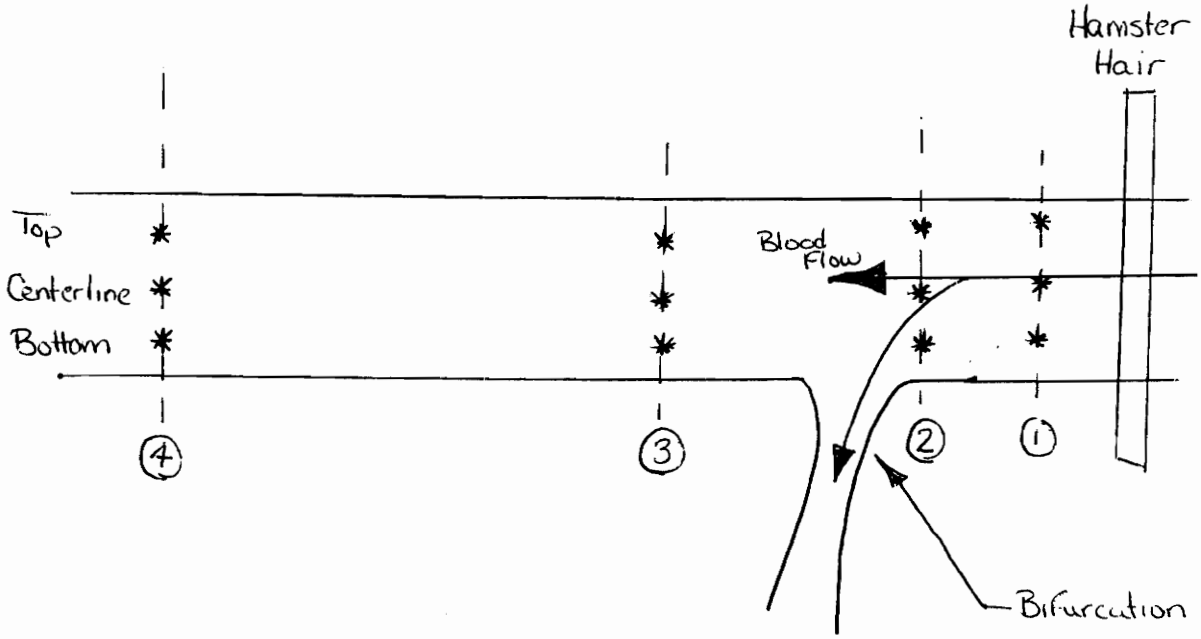

Fig. 22 Top view of hamster arteriole, hamster hair was used as a locational landmark. (Top, Centerline and Bottom denote the regions in which measurements were made) (* indicates the approximate location of measurement within the given region)

the Hb solution experiment, needed to calculate optical densities. To approximate this, an avascular region is imaged which is adjacent to the arteriole being measured. Caution should be exhibited here not to choose an avascular region which contains vessels out of the plane of focus. These data are also used in the calculations of the ratios of intensity at each isosbestic wavelength relative to the oxygen dependent wavelength; k_1 and k_2:

$$k_1 = \frac{I_{0,549}}{I_{0,560}}$$

$$k_2 = \frac{I_{0,523}}{I_{0,560}} \qquad (5.5\text{-}6)$$

These ratios tend to remain constant over a given tissue region, however, it is best to take new readings at each new measurement site.

When recording images for subsequent analysis, the illumination (KV and gain setting for the SIT camera) should remain constant for each measuring region. Altering these settings could change the black level of the SIT camera. This black level is pertinent as it is subtracted from each intensity (gray scale) value prior to using it in the calculations for optical densities.

After all of the necessary triplicated images are recorded, the recording is utilized in conjunction with the

IMAGELAB analysis software. As was performed in the Hb experiment, images are captured and stored, Fig. 23. Intensity values are then obtained across the microvessel at each measuring site of Fig. 22. Landmarks on the microvessel walls were utilized when digitizing to assure that intensity values at each of the three wavelengths were being retrieved from the same vessel location.

In obtaining values for I_o, an avascular region was chosen and several pixels in that region were digitized. An average of these pixel intensity values was calculated and used as the I_o value.

Once all of the measuring sites were digitized and the intensity values recorded, the calculations to obtain the SO_2 profile were performed.

5.7 Experimental Conclusions

Using the video microscopy system described above for the in vivo measurements proved to be quite manageable. Developing a systematic method to record beneficial images along the arteriole was the most difficult step. As is the case in most experimental research, the more experiments performed, the easier the experiment is to perform, and the more accurate the results.

The image analysis system was difficult to use. Not being able to acquire the intensity values used to create the graph illustrated in Fig. 17 made the data retrieval process

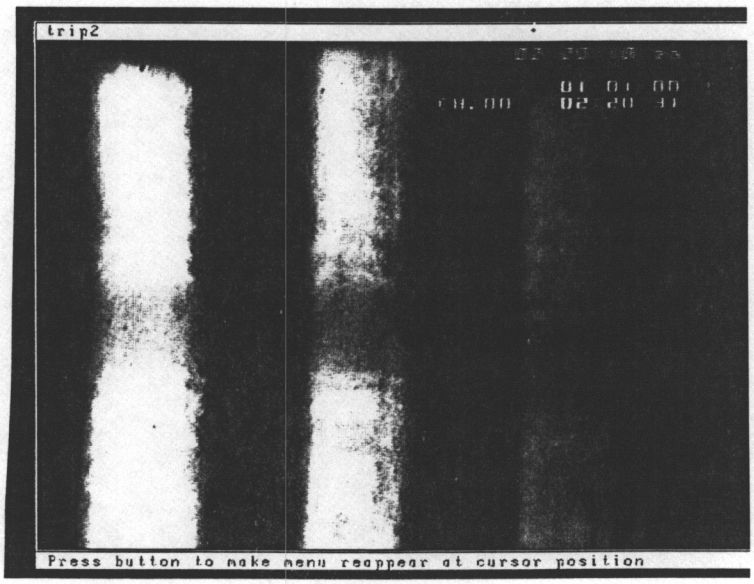

Fig. 23 Example of triplicated image of an arteriole in a hamster retractor muscle.

toilsome. Using the mouse, the cursor was placed on a pixel, the gray scale value was displayed on the screen and that value was hand recorded for subsequent analysis. To improve analysis procedures, a more efficient image analysis software should be utilized or incorporating an on-line data retrieval system into the video microscopy system would be favorable.

6.0 CALCULATIONS AND RESULTS

6.1 Introduction

The method outlined in section 2.4 was utilized to calculate oxygen saturation values in an arteriole in a hamster retractor muscle. Several sites were measured, three of them surrounding a bifurcation, one site was approximately five diameters downstream from the bifurcation. The last measurement was one performed as a control value. This was a measurement performed while the hamster was breathing 100% oxygen, hence, the SO_2 should be 100%.

The optical triplicator appeared to function as designed. The image at 523 nm was downshifted approximately 20 pixels on the monitor. This was compensated for during image processing.

The following sections will review the data collected, and the calculation results for both the in vitro and in vivo experiments.

6.2 Hemoglobin Solution Results

As described in section 5.5, a deoxyhemoglobin and an oxyhemoglobin solution were prepared. These, along with a distilled water sample, were placed in 100 μm path length microslides. The approximate concentration of the hemoglobin was 10 mM (milli Molar). This value is based on the dilution of RBC's in distilled water.

The microscopy system was set up to use the conventional

chart recorder as the data collection method. A 20% neutral density filter was placed in the path of the incident light for the distilled water sample. This reduced the intensity so not to saturate the video camera. Each sample was viewed at a 20X magnification.

The isosbesticity of the 549 and 523 nm filters were checked. Recall, isosbesticity is required so that the same linear relationship between SO_2 and $(OD_{560}-B)/(OD_{549}-B)$ for blood and SO_2 and OD_{560}/OD_{549} for Hb solutions can be obtained. Using the data collected from the chart recorder, the optical density at 549 and 523 nm for both the oxy- (i.e. S=100) and deoxyhemoglobin (i.e. S=0) was calculated:

$$\frac{OD_{549}(S=0)}{OD_{549}(S=100)}=1.057$$

$$\frac{OD_{523}(S=0)}{OD_{523}(S=100)}=1.049 \qquad (6.2\text{-}1)$$

Exact isosbesticity occurs when these ratios equal 1.000. Within the margin of experimental error, the filters can be assumed to be isosbestic and oxygen saturation can be calculated based on a linear response.

Following this, the constants to be used in the in vivo calculations were determined. A ρ value for the oxy- and deoxyhemoglobin solutions was calculated:

$$\rho_1 = 1.589$$

$$\rho_0 = 1.602$$

(6.2-2)

These values were then averaged to yield an overall ρ value of 1.595, slightly lower that the theoretical "book" value of 1.941. This value was however used for the in vivo calculation.

The values for R_1 and R_0 used to calculate m and b were measured to be 0.720 and 1.080, respectively. Hence the calculated values for m and b were:

$$m = -2.778$$

$$b = 3.000$$

(6.2-3)

The "book" values here are m=-2.915 and b=2.983, again slightly different from the above calculated values.

6.3 Diameter Calculations of Retractor Muscle Arteriole

Following the preparation of the hamster retractor muscle and searching for an "optically clear" arteriole, according to section 5.6, the in vivo experiment was ready to begin. The hamster chosen was approximately 52 days old, weighed 82 grams and had very little connective tissue.

The first step in determining the vessel diameter was to determine the conversion factor for number of pixels to microns. This was accomplished by using an image of a stage

micrometer. Using the image processing system it was determined that 48.75 ± 0.96 pixels was equivalent to 10 μm at a 50X magnification. Pixel measurements were then made at each of the measuring sites, the diameter results are listed in Table 3.

6.4 Hamster Retractor Muscle Oxygen Saturation Calculations

Figure 22 previously described in chapter 5 is a schematic of the arteriole measured and the approximate location of each measurement site. The hamster hair shown in the drawing was the location landmark used.

Beginning with site 1, upstream of the bifurcation, measurements were made in three regions of the vessel, the top, along the centerline and in the bottom region. The I_o values were measured from an avascular region just above the vessel. Forty measurements were made at each of the three wavelengths in each vessel region. This data is listed in Table 4. As can be seen, the first standard deviations of the transmitted intensity values are small, therefore, indicating the measurements are precise. However, the deviations on the I_o values are significantly greater, indicating the difficulty in finding a uniform avascular region to measure. Hence, the k_1 and k_2 values calculated show more variation that one would like:

Table 3. Diameter of Hamster Arteriole

Measuring Sites	Diameter (μm)
1	52.72 ± 0.02
2	52.92 ± 0.02
3	51.07 ± 0.03
4	51.42 ± 0.02

TABLE 4 INTENSITY DATA FOR MEASUREMENT SITE 1

SITE 1

	560	std	549	std	523	std
Top	102.57	4.63	62.19	3.08	28.76	2.99
Mid	76.74	3.35	42.55	3.64	24.04	3.47
Btm	94.17	7.30	57.48	3.76	32.17	2.23

	I_o	std
560	184.06	9.44
549	127.65	11.44
523	47.47	18.50

$$k_1 = 0.69 \pm 0.07$$

$$k_2 = 0.26 \pm 0.10$$

(6.4-1)

The oxygen saturation values were then calculated using the above values for k_1 and k_2:

$$SO_2(T) = 86.09 \pm 5.67\%$$

$$SO_2(Ctrline) = 77.65 \pm 3.73\%$$

$$SO_2(Btm) = 54.57 \pm 2.88\%$$

(6.4-2)

The location of measuring site 2 was on the upstream edge of the bifurcation. The I_o values were measured from what appeared to be a uniform region just below the vessel. The location along the vessel diameter and the number of measurements taken were performed the same as at site 1. The data are listed in Table 5.

Again, the standard deviations were higher for the I_o values than they were for the transmitted intensity values. The calculated k_1 and k_2 values are:

$$k_1 = 0.66 \pm 0.08$$

$$k_2 = 0.27 \pm 0.03$$

(6.4-3)

These give rise to the foloowing oxygen saturation values:

TABLE 5 INTENSITY DATA FOR MEASUREMENT SITE 2

SITE 2

	560	std	549	std	523	std
Top	71.83	6.03	45.74	4.13	20.38	2.77
Mid	53.21	5.12	33.21	2.88	17.38	1.59
Btm	71.69	5.07	44.48	4.12	24.88	2.81

	I_o	std
560	203.76	15.86
549	134.06	11.49
523	55.98	5.48

$$SO_2(T) = 74.39 \pm 20.24\%$$

$$SO_2(Ctrline) = 46.41 \pm 4.71\%$$

$$SO_2(Btm) = 42.99 \pm 4.20\%$$

(6.4-4)

Measuring site 3 was located just downstream of the bifurcation. The I_o values here were measured from a region just above the vessel. The data are listed in Table 6. The calculated k_1 and k_2 values are:

$$k_1 = 0.68 \pm 0.10$$

$$k_2 = 0.27 \pm 0.05$$

(6.4-5)

And, the oxygen saturation values are:

$$SO_2(T) = 90.74 \pm 7.32\%$$

$$SO_2(Ctrline) = 73.07 \pm 5.58\%$$

$$SO_2(Btm) = 61.88 \pm 3.30\%$$

(6.4-6)

Measuring site 4 was located approximately five diameters downstream from the bifurcation. Here, the avascular region chosen was below the vessel. The data are listed in Table 7. The calculated k_1 and k_2 values are:

$$k_1 = 0.67 \pm 0.06$$

$$k_2 = 0.27 \pm 0.03$$

(6.4-7)

TABLE 6 INTENSITY DATA AT MEASUREMENT SITE 3

SITE 3

	560	std	549	std	523	std
Top	73.07	3.51	44.79	3.57	21.24	2.63
Mid	55.29	3.99	33.05	2.75	17.48	2.85
Btm	69.67	3.99	41.26	4.38	24.17	2.64

	I_o	std
560	167.59	17.35
549	114.71	10.81
523	46.04	4.84

TABLE 7 INTENSITY DATA AT MEASUREMENT SITE 4

SITE 4

	560	std	549	std	523	std
Top	54.36	4.22	33.86	3.94	16.67	2.65
Mid	33.43	4.19	15.57	3.23	10.48	2.62
Btm	49.79	4.55	27.93	3.02	17.86	2.58

	I_o	std
560	131.59	8.40
549	88.46	6.32
523	35.68	3.81

Hence, the oxygen saturation values are:

$$SO_2(T) = 61.84 \pm 7.75\%$$

$$SO_2(Ctrline) = 96.46 \pm 4.46\%$$

$$SO_2(Btm) = 62.90 \pm 3.08\%$$

(6.4-8)

The last measurement was performed at the location of measurement site 2. However, this experiment was performed with the hamster breathing 100% O_2. The I_o values were again measured below the vessel. For this measurement, values were taken only along the centerline of the vessel, Table 8. The calculated k_1 and k_2 values are:

$$k_1 = 0.70 \pm 0.06$$

$$k_2 = 0.29 \pm 0.03$$

(6.4-9)

And, as expected, the oxygen saturation is:

$$SO_2(Ctrline) = 107.26 \pm 4.51\%$$

(6.4-10)

To determine the oxygen saturation variation, the non-linear equations ($(OD_{560} - B)$ and $(OD_{549} - B)$) were normalized and a program was written to calculate the errors. The program is listed in appendix A.

6.5 Conclusions

As discussed previously, the most critical portion of the

TABLE 8 INTENSITY DATA FOR HAMSTER BREATHING 100% O_2

SITE 5

	560	std	549	std	523	std
Top	----	----	----	----	----	----
Mid	51.74	3.47	28.26	3.54	16.00	2.34
Btm	----	----	----	----	----	----

	I_o	std
560	195.75	10.33
549	136.60	9.37
523	57.38	4.17

experiment is the determination of k_1 and k_2. Ideally this would be determined for the vessel under study when it is RBC free (i.e. plasma only). Since this is impossible to achieve in vivo, uniform avascular regions are measured. This technique is not precise but is a "best estimate" of the incident intensity. As the data above show, k_1 ranged from 0.66 to 0.70 and k_2 ranged from 0.26 to 0.29. Although these ranges are small and the errors on each values were generally only ±0.01, the logarithmic function in the oxygen saturation calculation magnifies the smallest deviations.

Swain and Pittman (15) predicted oxygen saturation values for arterioles in the hamster retractor muscle. For a second order vessel (i.e. approximately 50 μm) oxygen saturations should fall in the 60 - 70% range. Some of the values calculated here were above this range and some were below. However, considering the errors associated with each and the fact that this was only one hamster measurement, the data are remarkably accurate. One other consideration is the different experimental procedures. Swain and Pittman performed their measurements using the system where fiber optic leads were coupled to photomultiplier tubes (8) while these measurements were performed with the improved optical triplicator.

Figure 24 illustrates the oxygen saturation profiles obtained at the different measuring sites. It can be seen that for sites 1, 2, and 3, the oxygen saturation is highest

Fig. 24 Oxygen Saturation Profile

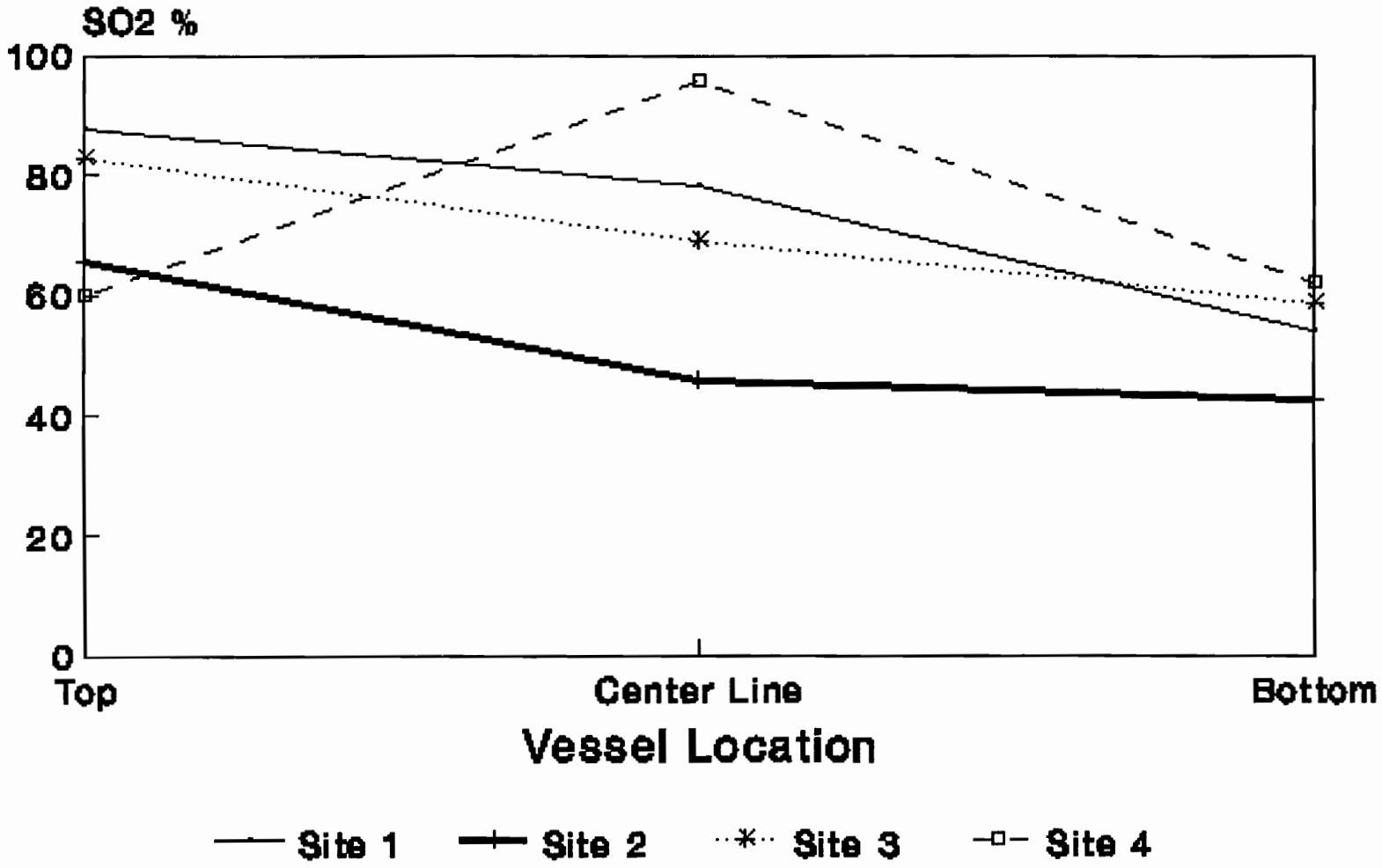

Note: Error bars omitted for clarity

in the top region of the vessel. On the other hand, site 4 shows the highest oxygen saturation along the centerline. This oxygen saturation variation can be explained by the locations of the measurement sites. Sites 1, 2, and 3 border a bifurcation which introduces asymmetry and possible mixing of the blood. Site 4 is downstream, away from any bifurcations, therefore, the flow is expected to be more uniform.

Although several in vivo experiments were performed, only the one documented here was accurate. The other experiments were not a loss. They were learning experiments which helped to fine tune the system to achieve the accuracy which this experiment shows. Now that the system has been refined, to achieve more accurate oxygen saturation values and a more complete representation of the profile, more hamsters should be studied. It would also be advantageous to take measurements in more regions across the vessel diameter. Time constraints limited the author to studying data from only one hamster, and, it is hoped that this research will continue in the hands of another inspired researcher.

7.0 CONCLUSIONS AND FUTURE WORK

7.1 Introduction

This project was undertaken to improve the measurement techniques of photometric microscopy. An optical triplicator was designed, fabricated and used with the microscopy system. It was shown that with this assembly, oxygen saturation values could be obtained. The eventual goal is to use this system to determine the diffusive loss of oxygen over a given length of vessel. Determining oxygen saturation is the first step toward this goal. With time, this system can be used to determine the other variables involved in calculating diffusive loss of oxygen such as: average blood velocity, hemoglobin concentration, and the amount of oxygen that can bind to hemoglobin.

7.2 Observation and Recommendations

Throughout the entire project, details were noted which would improve the function of the system, hence the accuracy of the values obtained.

In the optical triplicator design, using non-polarizing beamsplitters would eliminate the polarization effects present in the triplicator. This may result in increasing the resolution of the system. A longer length of vessel could be observed if the slits were to be opened to 2.0 mm instead of the 1.5 mm now used.

It would be advantageous to equalize the intensities of

the three images. This could be achieved by placing neutral density filters in the paths of images A and B. Then, with equal intensities the kilovolts and gain adjustments on the video camera could be increased to enhance the contrast and the clarity of the image. Without these filters, the kilovolts and gain adjustments need to remain low so as not to saturate the video camera.

The design of the housing could be made more accessible. This would allow for cleaning of the optics, adjusting the optics and additions such as the neutral density filters to be made easily. Along a similar line, to improve the alignment of the images on the monitor, another optical adhesive should be explored. The characteristics should be: a long working life, low viscosity, and strong enough prior to curing to hold the beamsplitters and prisms on their respective mounts while the triplicator is in its operating position.

The image processing system used appeared to be inferior to the capabilities of computers today. It was suitable for determining intensities (gray scale values) pixel by pixel. However, it would be best if a system could give an average value over many pixels. The choice system would be one which was incorporated with a program to compute oxygen saturation values. A superior system would be one that was on line and able to be used in real time.

The measurement error inherent in the system should be

determined. To accomplish this, a system of experiments using hemoglobin solutions of the same concentration could be used. Several measurements should be made at each wavelength, by different operators, at different times. This would eliminate any subjectivity and factor in any "noise" which may be present. Once these measurements are made, the overall measurement error can be assessed.

Finally, due to the sensitivity of k_1 and k_2 on the final oxygen saturation value, a more accurate method to determine the I_o values should be designed. Due to the difficult nature of determining these values in vivo, possibly a system could be assembled which modeled the in vivo characteristics. Once this model is proven, the values determined could be used for all measurements done in vivo.

7.3 Conclusions

Concisely summarizing the previous discussions and noting possible extensions:

- Optical triplicator operates satisfactorily with high resolution and precise image alignment
- Oxygen saturation values obtained were in the predicted range
- Oxygen saturation profiles showed to be non-uniform around the asymmetric bifurcation and uniform in regions away from all bifurcations
- Project should be extended to determining the diffusive

loss of oxygen in the microvascular network

- Other applications outside of the biomedical field which may have needs for triplicated monochromatic images should be investigated
- Beam splitters should be replaced with non-polarizing beam splitters
- The slits inside the triplicator should be widened to allow for a longer vessel length to be viewed
- Neutral density filters should be placed in the optical path of images A and B to equalize the intensities of all of the images
- The triplicator housing should be made more accessible to accommodate change easier
- An improved optical adhesive should be used to place the optical elements, therefore improving the alignment
- A real time image processing system with on line computational abilities should be developed
- An experiment should be set up and run to determine the measurement error inherent in the assembly
- A new superior method for determining the incident intensities (hence, k_1 and k_2) should be developed

REFERENCES

1. Krogh, A.; *The Anatomy and Physiology of Capillaries*, Yale University Press, New Haven, 1929.

2. Davies, P.; Bronk, D.: Oxygen tension in mammalian brain. Fed. Proc. 16:689-692, 1957.

3. Pittman, R.; Duling, B.; "Effects of Altered Carbon Dioxide Tension on Hemoglobin Oxygenation in Hamster Cheek Pouch," *Microvas. Rec.* 13:211-224, 1977.

4. Lipowsky, H.; Usami, S.; Chien, S.; Pittman, R.; "Hematocrit Determination in Small Bore Tubes by Differential Spectrophotometry," *Microvas. Rec.* 24:42-45, 1982.

5. Pittman, R.; Duling, B.; "A New Method for the Measurement of Percent Oxyhemoglobin," *J. Appl. Physiol.* 38:315-320, 1975.

6. Pittman, R.; Duling, B.; "Measurement of Percent Oxyhemoglobin in the Microvasculature;" *J. Appl. Physiol.* 38:321-327, 1975.

7. Ellsworth, M.; Pittman, R.; "Evaluation of Photometric Methods for Quantifying Convective Mass Transport in Microvessels," *Am. J. Physiol.* 251 (*Heart Circ. Physiol. 20*): H869-H879, 1987.

8. Duling, B.; Damon, D; Donaldson, S.; Pittman, R.; "A Computerized System for the Densitometric Analysis of the Microcirculation," *J. Appl. Physiol.* 55:642-651, 1983.

9. Pittman, R.; "Microvessel Blood Oxygen Measurement Techniques," *Microcirculatory Technology*, Academic Press, 1986.

10. Kramer, K.; Elam, J. D.; Saxton, G.A.; Elam, W.N., Jr.: "Influence of Oxygen Saturation, Erythrocyte Concentration, and Optical Depth Upon the Red and Near-Infrared Light Transmittance of Whole Blood," *Am. J. Physiol.* 165:229-246, 1951.

11. Twersky, V.; "Interface Effects in Multiple Scattering by Large, Low-Refracting Absorbing Particles," *J. Opt. Soc. Am.* 60:908-914, 1970.

12. Van Assendelft, O. W., "Spectrophotometry of Haemoglobin Derivatives," Thomas, Springfield, Illinois, 1970.

13. Howling, D. H.; Fitzergerald, P. J.; "The Nature, Significance, and Evaluation of the Schwarzschild-Villiger (SV) Effect in Photometric Procedures," *J. Biophys. Biochem. Cytol.* 6:313-337, 1959.

14. Sullivan, S. M.; Pittman, R.; "Hamster Retractor Muscle: A New Preparation for Intravital Microscopy," *Microvas. Rec.* 23:329-335, 1982.

15. Swain, D.; Pittman, R.; "Oxygen Exchange in the Micro-Circulation of Hamster Retractor Muscle," *Am. J. Physiol.* 256 (Heart Circ. Physiol 25): H247-H255, 1989.

16. Hecht, E.; *Optics*, Addison-Wesley Publishing Company, Inc., 1987.

17. Guyton, A. C., M.D.; *Textbook of Medical Physiology*, W.B. Saunders Company, 1991.

APPENDIX A

ERROR ANALYSIS PROGRAM

```
      real k1,k2,m
      DATA R,M,B/1.595,-2.778,3.0/
      ef = alog10(2.7183)
      open (1,file='mott.dat',status='unknown')
      open (2,file='mott.out')
      do 1 iii=1,4
      read (1,100) name
100   format(a2)
      read (1,101) xo523,eo523,xo549,eo549,xo560,e0560
101   format(6f7.2)
      k1=xo549/xo560
      k2=xo523/xo560
      EZ1=(eo549**2+eo560**2*k1**2)/xo560**2
      Ek1=SQRT(EZ1)
      EZ2=(EO523**2+EO560**2*k2**2)/xo560**2
      Ek2=SQRT(EZ2)
      WRITE(*,102) NAME,xo523,eo523,xo549,eo549,xo560,eo560,
     *k1,Ek1,k2,Ek2
      WRITE(2,102) NAME,xo523,eo523,xo549,eo549,xo560,eo560
     *k1,Ek1,k2,Ek2
102   FORMAT(//' Site ',A2,2(/' Input',3(F7.2,'+-,f6.2,3x)))

      do 2 ii-1,3
      read (1,101) x523,e523,x549,e549,x560,e560
      WRITE(*,103) ii,x523,e523,x549,e549,x560,e560
      WRITE(2,103) ii,x523,e523,x549,e549,x560,e560
103   FORMAT(/' Pass '/i1,2(f7.2,'+-',F6.2,3x))
104   FORMAT(' Output',3(f7.2"+-'f6.2,3x))
      Y = (R*ALOG10(k2/X523)-ALOG10(k1/X549))/(R-1.0)
      o560 = -ALOG10(x560) - Y
      o549 = ALOG10(k1/X549) - Y
      so = ((M*o560/o549)+B)*100.
      ey=(R**2*(EZ2+(e523/x523)**2)+EZ1+(E549/x549)**2)/(R-
1.)**2
      Eo560=SQRT(ef**2*((E560/X560)**2+ey)
      Eo549=SQRT(ef**2*((E549/X549)**2+EZ1)+ey)
      eso=sqrt(m**2*((Eo560/o549)**2+(o560*Eo549/o549**2)
**2))
      WRITE(*,104) o560,eo560,o549,eo549,so,eso
      WRITE(2,104) o560,eo560,o549,eo549,so,eso
2     continue
      pause

1     continue
      close(1)
      close(2)
      END
```

VITA

Elizabeth Ann Mott was born in Auburn, New York to Mr. and Mrs. Bertrand W. Mott. She completed her secondary education at Jordan-Elbridge Jr. Sr. High School in New York and went on to Alfred University, Alfred, New York. There she received a bachelor's degree in Ceramic Engineering with a minor in Coaching in 1990. The next step was to earn a master's degree in Electrical Engineering at Virginia Tech in 1992. Elizabeth plans to continue working as a Biomedical Engineer at Galileo Electro-Optics, Inc. in Forest, Virginia.